

17. Toyoshiba H, Yamanaka T, Sone H *et al.* Gene interaction network suggests dioxin induces a significant linkage between aryl hydrocarbon receptor and retinoic acid receptor beta. *Environ Health Perspect* 2004; **112**: 1217–1224.
18. Bumgarner RE, Yeung KY. Methods for the inference of biological pathways and networks. *Methods Mol Biol* 2009; **541**: 225–245.
19. Huang JC, Babak T, Corson TW *et al.* Using expression profiling data to identify human microRNA targets. *Nat Methods* 2007; **4**: 1045–1049.
20. Li H, Lu L, Manly KF *et al.* Inferring gene transcriptional modulatory relations: a genetical genomics approach. *Hum Mol Genet* 2005; **14**: 1119–1125.
21. Toyokuni S. Molecular mechanisms of oxidative stress-induced carcinogenesis: from epidemiology to oxigenomics. *IUBMB Life* 2008; **60**: 441–447.
22. Kultz D. Molecular and evolutionary basis of the cellular stress response. *Annu Rev Physiol* 2005; **67**: 225–257.
23. Hamilton ML, Van Remmen H, Drake JA *et al.* Does oxidative damage to DNA increase with age? *Proc Natl Acad Sci USA* 2001; **98**: 10469–10474.
24. von Zglimicki T, Saretzki G, Ladhoff J, d'Adda di Fagagna F, Jackson SP. Human cell senescence as a DNA damage response. *Mech Ageing Dev* 2005; **126**: 111–117.
25. Lambeth JD. Nox enzymes, ROS, and chronic disease: an example of antagonistic pleiotropy. *Free Radic Biol Med* 2007; **43**: 332–347.
26. Collado M, Blasco MA, Serrano M. Cellular senescence in cancer and aging. *Cell* 2007; **130**: 223–233.
27. Trachootham D, Alexandre J, Huang P. Targeting cancer cells by ROS-mediated mechanisms: a radical therapeutic approach? *Nat Rev Drug Discov* 2009; **8**: 579–591.
28. Kimbro KS, Simons JW. Hypoxia-inducible factor-1 in human breast and prostate cancer. *Endocr Relat Cancer* 2006; **13**: 739–749.
29. Kruse JP, Gu W. Modes of p53 regulation. *Cell* 2009; **137**: 609–622.
30. Benz CC, Yau C. Ageing, oxidative stress and cancer: paradigms in parallax. *Nat Rev Cancer* 2008; **8**: 875–879.
31. Vousden KH, Ryan KM. p53 and metabolism. *Nat Rev Cancer* 2009; **9**: 691–700.
32. Capri M, Salvioli S, Sevini F *et al.* The genetics of human longevity. *Ann NY Acad Sci* 2006; **1067**: 252–263.
33. Sanchez-Capelo A. Dual role for TGF-beta1 in apoptosis. *Cytokine Growth Factor Rev* 2005; **16**: 15–34.
34. Chalmers L, Kaskel FJ, Bamgola O. The role of obesity and its biochemical correlates in the progression of chronic kidney disease. *Adv Chronic Kidney Dis* 2006; **13**: 352–364.
35. Eleuteri E, Magno F, Gnemmi I *et al.* Role of oxidative and nitrosative stress biomarkers in chronic heart failure. *Front Biosci* 2009; **14**: 2230–2237.
36. Albano E. Oxidative mechanisms in the pathogenesis of alcoholic liver disease. *Mol Aspects Med* 2008; **29**: 9–16.
37. Vogelstein B, Lane D, Levine AJ. Surfing the p53 network. *Nature* 2000; **408**: 307–310.
38. Vousden KH, Lane DP. p53 in health and disease. *Nat Rev Mol Cell Biol* 2007; **8**: 275–283.
39. Marchenko ND, Moll UM. The role of ubiquitination in the direct mitochondrial death program of p53. *Cell Cycle* 2007; **6**: 1718–1723.
40. Chao C, Wu Z, Mazur SJ *et al.* Acetylation of mouse p53 at lysine 317 negatively regulates p53 apoptotic activities after DNA damage. *Mol Cell Biol* 2006; **26**: 6859–6869.
41. Chao C, Herr D, Chun J, Xu Y. Ser18 and 23 phosphorylation is required for p53-dependent apoptosis and tumor suppression. *EMBO J* 2006; **25**: 2615–2622.
42. Blattner C, Tobiasch E, Litfen M, Rahmsdorf HJ, Herrlich P. DNA damage induced p53 stabilization: no indication for an involvement of p53 phosphorylation. *Oncogene* 1999; **18**: 1723–1732.
43. Chao C, Hergenbahn M, Kaeser MD *et al.* Cell type- and promoter-specific roles of Ser18 phosphorylation in regulating p53 responses. *J Biol Chem* 2003; **278**: 41028–41033.
44. Brooks CL, Gu W. Ubiquitination, phosphorylation and acetylation: the molecular basis for p53 regulation. *Curr Opin Cell Biol* 2003; **15**: 164–171.
45. Poyton RO, Ball KA, Castello PR. Mitochondrial generation of free radicals and hypoxic signaling. *Trends Endocrinol Metab* 2009; **20**: 332–340.
46. van Faassen EE, Bahrami S, Feelisch M *et al.* Nitrite as regulator of hypoxic signaling in mammalian physiology. *Med Res Rev* 2009; **29**: 683–741.
47. Taylor CT, Cummins EP. The role of NF-kappaB in hypoxia-induced gene expression. *Ann NY Acad Sci* 2009; **1177**: 178–184.
48. Maziere C, Maziere JC. Activation of transcription factors and gene expression by oxidized low-density lipoprotein. *Free Radic Biol Med* 2009; **46**: 127–137.
49. Bertout JA, Majmundar AJ, Gordan JD *et al.* HIF2alpha inhibition promotes p53 pathway activity, tumor cell death, and radiation responses. *Proc Natl Acad Sci USA* 2009; **106**: 14391–14396.
50. Moriya J, Minamoto T, Tateno K *et al.* Inhibition of semaphorin as a novel strategy for therapeutic angiogenesis. *Circ Res* 2010; **106**: 391–398.
51. Fosslien E. Cancer morphogenesis: role of mitochondrial failure. *Ann Clin Lab Sci* 2008; **38**: 307–329.
52. Koli K, Myllarniemi M, Keski-Oja J, Kinnula VL. Transforming growth factor-beta activation in the lung: focus on fibrosis and reactive oxygen species. *Antioxid Redox Signal* 2008; **10**: 333–342.
53. Zhang H, Jiang Z, Chang J *et al.* Role of NAD(P)H oxidase in transforming growth factor-beta1-induced monocyte chemoattractant protein-1 and interleukin-6 expression in rat renal tubular epithelial cells. *Nephrology (Carlton)* 2009; **14**: 302–310.
54. Chan DW, Liu VW, To RM *et al.* Overexpression of FOXG1 contributes to TGF-beta resistance through inhibition of p21WAF1/CIP1 expression in ovarian cancer. *Br J Cancer* 2009; **101**: 1433–1443.
55. Tezel G. TNF-alpha signaling in glaucomatous neurodegeneration. *Prog Brain Res* 2008; **173**: 409–421.
56. Aguilera-Aguirre L, Basci A, Saavedra-Molina A, Kurosky A, Sur S, Boldogh I. Mitochondrial dysfunction increases allergic airway inflammation. *J Immunol* 2009; **183**: 5379–5387.
57. Bertram KM, Bagloli CJ, Phipps RP, Libby RT. Molecular regulation of cigarette-smoke induced-oxidative stress in human retinal pigment epithelial cells: implications for age-related macular degeneration. *Am J Physiol* 2009; **297**: C1200–C1210.
58. Lal N, Kumar J, Erdahl WE *et al.* Differential effects of non-steroidal anti-inflammatory drugs on mitochondrial dysfunction during oxidative stress. *Arch Biochem Biophys* 2009; **490**: 1–8.
59. Nelson GM, Ahlborn GJ, Allen JW *et al.* Transcriptional changes associated with reduced spontaneous liver tumor incidence in mice chronically exposed to high dose arsenic. *Toxicology* 2009; **266**: 6–15.
60. Bailey SM. A review of the role of reactive oxygen and nitrogen species in alcohol-induced mitochondrial dysfunction. *Free Radic Res* 2003; **37**: 585–596.
61. Kim GJ, Chandrasekaran K, Morgan WF. Mitochondrial dysfunction, persistently elevated levels of reactive oxygen species and radiation-induced genomic instability: a review. *Mutagenesis* 2006; **21**: 361–367.
62. Protti A, Singer M. Bench-to bedside review: potential strategies to protect or reverse mitochondrial dysfunction in sepsis-induced organ failure. *Crit Care* 2006; **10**: 228.
63. Shults CW. Mitochondrial dysfunction and possible treatments in Parkinson's disease – a review. *Mitochondrion* 2004; **4**: 641–648.
64. Lee HK, Cho YM, Kwak SH, Lim S, Park KS, Shim EB. Mitochondrial dysfunction and metabolic syndrome-looking for environmental factors. *Biochim Biophys Acta* 2010; **1800**: 282–289.
65. Almon RR, Lai W, DuBois DC, Jusko WJ. Corticosteroid-regulated genes in rat kidney: mining time series array data. *Am J Physiol* 2005; **289**: E870–E882.
66. Jin JY, Almon RR, DuBois DC, Jusko WJ. Modeling of corticosteroid pharmacogenomics in rat liver using gene microarrays. *J Pharmacol Exp Ther* 2003; **307**: 93–109.
67. Sullivan CJ, Teal TH, Luttrell IP, Tran KB, Peters MA, Wessells H. Microarray analysis reveals novel gene expression changes associated with erectile dysfunction in diabetic rats. *Physiol Genomics* 2005; **23**: 192–205.
68. Lattanzi W, Bernardini C, Gangitano C, Michetti F. Hypoxia-like transcriptional activation in TMT-induced degeneration: microarray expression analysis on PC12 cells. *J Neurochem* 2007; **100**: 1688–1702.
69. Erlandsen SE, Fykse V, Waldum HL, Sandvik AK. Octreotide induces apoptosis in the oxyntic mucosa. *Mol Cell Endocrinol* 2007; **264**: 188–196.
70. Chen H, Huang XN, Stewart AF, Sepulveda JL. Gene expression changes associated with fibronectin-induced cardiac myocyte hypertrophy. *Physiol Genomics* 2004; **18**: 273–283.

71. Guan H, Arany E, van Beek JP *et al.* Adipose tissue gene expression profiling reveals distinct molecular pathways that define visceral adiposity in offspring of maternal protein-restricted rats. *Am J Physiol* 2005; **288**: E663–E673.
72. Sakurai H, Bush KT, Nigam SK. Heregulin induces glial cell line-derived neurotrophic growth factor-independent, non-branching growth and differentiation of ureteric bud epithelia. *J Biol Chem* 2005; **280**: 42181–42187.
73. Koh S, Chung H, Xia H, Mahadevia A, Song Y. Environmental enrichment reverses the impaired exploratory behavior and altered gene expression induced by early-life seizures. *J Child Neurol* 2005; **20**: 796–802.
74. Kubisch CH, Gukovsky I, Lugea A *et al.* Long-term ethanol consumption alters pancreatic gene expression in rats: a possible connection to pancreatic injury. *Pancreas* 2006; **33**: 68–76.
75. Kodavanti UP, Schladweiler MC, Ledbetter AD *et al.* The spontaneously hypertensive rat: an experimental model of sulfur dioxide-induced airways disease. *Toxicol Sci* 2006; **94**: 193–205.
76. Bruder ED, Lee JJ, Widmaier EP, Raff H. Microarray and real-time PCR analysis of adrenal gland gene expression in the 7-day-old rat: effects of hypoxia from birth. *Physiol Genomics* 2007; **29**: 193–200.
77. Almon RR, DuBois DC, Yao Z, Hoffman EP, Ghimbovski S, Jusko WJ. Microarray analysis of the temporal response of skeletal muscle to methylprednisolone: comparative analysis of two dosing regimens. *Physiol Genomics* 2007; **30**: 282–299.
78. Chan MM, Lu X, Merchant FM, Iglehart JD, Miron PL. Gene expression profiling of NMU-induced rat mammary tumors: cross species comparison with human breast cancer. *Carcinogenesis* 2005; **26**: 1343–1353.
79. Kendzierski C, Irizarry RA, Chen KS, Haag JD, Gould MN. On the utility of pooling biological samples in microarray experiments. *Proc Natl Acad Sci USA*. 2005; **102**: 4252–4257.
80. Aplin AC, Gelati M, Fogel E, Carnevale E, Nicosia RF. Angiopoietin-1 and vascular endothelial growth factor induce expression of inflammatory cytokines before angiogenesis. *Physiol Genomics* 2006; **27**: 20–28.
81. Rampil IJ, Moller DH, Bell AH. Isoflurane modulates genomic expression in rat amygdala. *Anesth Analg* 2006; **102**: 1431–1438.
82. Collins JF. Gene chip analyses reveal differential genetic responses to iron deficiency in rat duodenum and jejunum. *Biol Res* 2006; **39**: 25–37.
83. Guzelian J, Barwick JL, Hunter L, Phang TL, Quattrochi LC, Guzelian PS. Identification of genes controlled by the pregnane X receptor by microarray analysis of mRNAs from pregnenolone 16 α -carbonitrile-treated rats. *Toxicol Sci* 2006; **94**: 379–387.
84. Gebel S, Gerstmayer B, Kuhl P, Borlak J, Meurrens K, Muller T. The kinetics of transcriptomic changes induced by cigarette smoke in rat lungs reveals a specific program of defense, inflammation, and circadian clock gene expression. *Toxicol Sci* 2006; **93**: 422–431.
85. Su Y, Simmen FA, Xiao R, Simmen RC. Expression profiling of rat mammary epithelial cells reveals candidate signaling pathways in dietary protection from mammary tumors. *Physiol Genomics* 2007; **30**: 8–16.
86. Rowe WB, Blalock EM, Chen KC *et al.* Hippocampal expression analyses reveal selective association of immediate-early, neuroenergetic, and myelinogenic pathways with cognitive impairment in aged rats. *J Neurosci* 2007; **27**: 3098–3110.
87. Volpicelli F, Caiazzo M, Greco D *et al.* Bdnf gene is a downstream target of Nurr1 transcription factor in rat midbrain neurons in vitro. *J Neurochem* 2007; **102**: 441–453.
88. Stemmer K, Ellinger-Ziegelbauer H, Ahr HJ, Dietrich DR. Carcinogen-specific gene expression profiles in short-term treated Eker and wild-type rats indicative of pathways involved in renal tumorigenesis. *Cancer Res* 2007; **67**: 4052–4068.
89. Impey S, McCorkle SR, Cha-Molstad H *et al.* Defining the CREB regulon: a genome-wide analysis of transcription factor regulatory regions. *Cell* 2004; **119**: 1041–1054.
90. Bush EW, Hood DB, Papst PJ *et al.* Canonical transient receptor potential channels promote cardiomyocyte hypertrophy through activation of calcineurin signaling. *J Biol Chem* 2006; **281**: 33487–33496.
91. Zhou Z, Cornelius CP, Eichner M, Bornemann A. Reinnervation-induced alterations in rat skeletal muscle. *Neurobiol Dis* 2006; **23**: 595–602.
92. Bursztyn M, Gross ML, Goltser-Dubner T, et al. Adult hypertension in intrauterine growth-restricted offspring of hyperinsulinemic rats: evidence of subtle renal damage. *Hypertension* 2006; **48**: 717–723.
93. Thomas H, Senkel S, Erdmann S *et al.* Pattern of genes influenced by conditional expression of the transcription factors HNF6, HNF4 α and HNF1 β in a pancreatic beta-cell line. *Nucleic Acids Res* 2004; **32**: e150.
94. Schumann A, Nutten S, Donnicola D *et al.* Neonatal antibiotic treatment alters gastrointestinal tract developmental gene expression and intestinal barrier transcriptome. *Physiol Genomics* 2005; **23**: 235–245.
95. Roy S, Khanna S, Kuhn DE *et al.* Transcriptome analysis of the ischemia-reperfused remodeling myocardium: temporal changes in inflammation and extracellular matrix. *Physiol Genomics*. 2006; **25**: 364–374.
96. Tugues S, Morales-Ruiz M, Fernandez-Varo G *et al.* Microarray analysis of endothelial differentially expressed genes in liver of cirrhotic rats. *Gastroenterology* 2005; **129**: 1686–1695.
97. Akavia UD, Shur I, Rechavi G, Benayahu D. Transcriptional profiling of mesenchymal stromal cells from young and old rats in response to Dexamethasone. *BMC Genomics* 2006; **7**: 95.
98. Zhou M, Roma A, Magi-Galluzzi C. The usefulness of immunohistochemical markers in the differential diagnosis of renal neoplasms. *Clin Lab Med* 2005; **25**: 247–257.
99. Schiffer D, Giordana MT, Mauro A, Migheli A, Germano I, Giaccone G. Immunohistochemical demonstration of vimentin in human cerebral tumors. *Acta Neuropathol* 1986; **70**: 209–219.
100. Niehans GA, Manivel JC, Copland GT, Scheithauer BW, Wick MR. Immunohistochemistry of germ cell and trophoblastic neoplasms. *Cancer* 1988; **62**: 1113–1123.
101. Iwakuma T, Lozano G. Crippling p53 activities via knock-in mutations in mouse models. *Oncogene* 2007; **26**: 2177–2184.
102. Marine JC, Jochemsen AG. Mdmx as an essential regulator of p53 activity. *Biochem Biophys Res Commun* 2005; **331**: 750–760.
103. Tang Y, Zhao W, Chen Y, Zhao Y, Gu W. Acetylation is indispensable for p53 activation. *Cell* 2008; **133**: 612–626.
104. Gong X, Kole L, Iskander K, Jaiswal AK. NRH:quinone oxidoreductase 2 and NAD(P)H:quinone oxidoreductase 1 protect tumor suppressor p53 against 20S proteasomal degradation leading to stabilization and activation of p53. *Cancer Res* 2007; **67**: 5380–5388.
105. Lai Z, Yang T, Kim YB *et al.* Differentiation of Hdm2-mediated p53 ubiquitination and Hdm2 autoubiquitination activity by small molecular weight inhibitors. *Proc Natl Acad Sci USA* 2002; **99**: 14734–14739.
106. Wang W, Ho WC, Dicker DT *et al.* Acridine derivatives activate p53 and induce tumor cell death through Bax. *Cancer Biol Ther* 2005; **4**: 893–898.
107. Kawata K, Yokoo H, Shimazaki R, Okabe S. Classification of heavy-metal toxicity by human DNA microarray analysis. *Environ Sci Technol* 2007; **41**: 3769–3774.
108. Fry RC, Navasumrit P, Valiathan C *et al.* Activation of inflammation/NF-kappaB signaling in infants born to arsenic-exposed mothers. *PLoS Genet* 2007; **3**: e207.
109. Chang L, Zhou B, Hu S *et al.* ATM-mediated serine 72 phosphorylation stabilizes ribonucleotide reductase small subunit p53R2 protein against MDM2 to DNA damage. *Proc Natl Acad Sci USA* 2008; **105**: 18519–18524.
110. Kollberg G, Darin N, Benan K *et al.* A novel homozygous RRM2B missense mutation in association with severe mtDNA depletion. *Neuromuscul Disord*. 2009; **19**: 147–150.
111. Liu X, Xue L, Yen Y. Redox property of ribonucleotide reductase small subunit M2 and p53R2. *Methods Mol Biol* 2008; **477**: 195–206.
112. Spinazzola A, Invernizzi F, Carrara F *et al.* Clinical and molecular features of mitochondrial DNA depletion syndromes. *J Inherit Metab Dis* 2009; **32**: 143–158.
113. Tyynismaa H, Suomalainen A. Mouse models of mitochondrial DNA defects and their relevance for human disease. *EMBO Rep* 2009; **10**: 137–143.
114. Ceryak S, Zingariello C, O'Brien T, Patierno SR. Induction of proapoptotic and cell cycle-inhibiting genes in chromium (VI)-treated human lung fibroblasts: lack of effect of ERK. *Mol Cell Biochem* 2004; **255**: 139–149.
115. Fanzo JC, Reaves SK, Cui L *et al.* Zinc status affects p53, gadd45, and c-fos expression and caspase-3 activity in human bronchial epithelial cells. *Am J Physiol* 2001; **281**: C751–C757.

116. Shih RS, Wong SH, Schoene NW, Lei KY. Suppression of Gadd45 alleviates the G2/M blockage and the enhanced phosphorylation of p53 and p38 in zinc supplemented normal human bronchial epithelial cells. *Exp Biol Med (Maywood)* 2008; **233**: 317–327.
117. Toyoshiba H, Sone H, Yamanaka T *et al.* Gene interaction network analysis suggests differences between high and low doses of acetaminophen. *Toxicol Appl Pharmacol* 2006; **215**: 306–316.
118. Yamanaka T, Toyoshiba H, Sone H, Parham FM, Portier CJ. The TAO-Gen algorithm for identifying gene interaction networks with application to SOS repair in *E. coli*. *Environ Health Perspect* 2004; **112**: 1614–1621.
119. Sone H, Imanishi S, Akanuma H *et al.* Gene expression signatures of environmental chemicals in cancer and in developmental disorders. In: Zhao BDM, Cadeans E. (eds) *The roles of free radicals in biology and medicine*. Beijing: Medimond, 2009; 45–52.
120. Chua PJ, Yip GW, Bay BH. Cell cycle arrest induced by hydrogen peroxide is associated with modulation of oxidative stress related genes in breast cancer cells. *Exp Biol Med (Maywood)* 2009; **234**: 1086–1094.
121. Feng XD, Huang SG, Shou JY *et al.* Analysis of pathway activity in primary tumors and NCI60 cell lines using gene expression profiling data. *Genomics Proteomics Bioinformatics* 2007; **5**: 15–24.

SUPPLEMENTAL MATERIALS

Supplement T1 – oxidative stress pathways

Categorical pathways	
Canonical pathway (orthology)	Gene name
Reactive oxygen species (ROS) metabolism and antioxidant defenses	
Glutathione peroxidases (GPx)	GPX1, GPX2, GPX3, GPX4, GPX5, GPX6, GPX7, GSTZ1
Peroxiredoxins (TPx)	PRDX1, PRDX2, PRDX3, PRDX4, PRDX5, PRDX6
Other peroxidases	CAT, CSDE1, CYGB, DUOX1, DUOX2, EPX, GPR156, LPO, MGST3, MPO, PIP3-E, PTGS1, PTGS2, PDXN, PDXNL, TPO, TTN
Other antioxidants	ALB, APOE, GSR, MT3, SELS, SRXN1, TXNDC2, TXNRD1, TXNRD2
Superoxide dismutases (SOD)	SOD1, SOD2, SOD3
Other genes involved in superoxide metabolism	ALOX12, CCS, CYBA, DUOX1, DUOX2, GTF2I, MT3, NCF1, NCF2, NOS2A, NOX5, PREX1, PRG3
Genes involved in ROS metabolism	AOX1, BNIP3, EPHX2, MPV17, SFTPD
Oxidative stress responsive genes	ANGPTL7, ATOX1, CAT, CCL5, CSDE1, DGKK, DHCR24, DUSP1, EPX, FOXM1, GLRX2, GPR156, GSS, KRT1, LPO, MBL2, MPO, MSRA, MTL5, NME5, NUDT1, OXR1, OXSR1, PDLIM1, PIP3-E, PNKP, PRDX2, PRDX5, PRDX6, PRNP, RNF7, SCARA3, SELS, SEPP1, SGK2, SIRT2, SRXN1, STK25, TPO, TTN
p53 signaling pathway	
Induction of apoptosis	BAX, BID, CDKN1A, CRADD, EI24, FADD, FASLG (TNFSF6), FOXO3, PCBP4, PRKCA, TNFRSF10B, TP53, TP73, TP73L
Anti-apoptosis	BCL2, BCL2A1, BIRC5, CASP2, HDAC1, IGF1R, MCL1, NFKB1, RELA, TNF, TNFRSF10
Other apoptosis genes	APAF1, BRCA1, CASP9, E2F1, GADD45A, GML, LRDD, P53AIP1, SIAH1, SIRT1, TP53BP2, TRAF2
Cell cycle arrest	CDKN1A, CDKN2A, CHEK1, CHEK2, GADD45A, GML, MYC, PCAF, PCBP4, RPRM, SESN1, SESN2
Cell cycle checkpoint	ATR, BRCA1, CCNE2, CCNG2, CDKN2A, RB1, TP53
Negative regulation of the cell cycle	BAX, BRCA1, CDKN2A, MSH2, NF1, PTEN, RB1, TP53, TP73, TP73L, TSC1, WT1
Regulation of the cell cycle	BRCA2, CDC2, CDC25A, CDK4, E2F1, E2F3, HK2, IGF1R, KRAS, PPM1D, PRKCA, STAT1, TADA3L, TP53BP2
Other cell cycle genes	BIRC5, CCNH, CCNB2, ESR1, MLH1, PCNA, PRC1
Negative regulation of cell proliferation	BAI1, BCL2, BTG2, CDKN1A, CDKN2A, CHEK1, GML, IFNB1, IL6, MDM2, MDM4, NF1, PCAF, PPM1D, SESN1
Positive regulation of cell proliferation	IGF1R, IL6
Cell Proliferation	BRCA1, CDC25A, CDC25C, CDK4, E2F1, MYC, PCNA, PRKCA
Cell growth and differentiation	ESR1, MCL1, MYOD1
Other genes related to cell growth, proliferation, and differentiation	EGR1, FOXO3A, JUN, KRAS, PTTG1
DNA repair genes	ATM, ATR, BRCA1, BTG2, CCNH, DNMT1, GADD45A, MSH2, PCNA, PTTG1, TP53, XRCC5
Human nitric oxide signaling pathway PCR array	
Genes with nitric-oxide synthase or oxidoreductase activity	NOS1, NOS2A, NOS3, NQO1
Positive regulators of nitric oxide biosynthesis	HSP90AB1 (HSPCB), INS
Negative regulators of nitric oxide biosynthesis	DNCL1, GLA, IL10
Other genes involved in NO biosynthesis	AKT1, ARG2, DDAH2, DNCL1, EGFR, GCH1, GCHFR

Genes induced by NO	CDKN1A, IL8, JUN, VEGFA
Genes suppressed by NO	CCNA1, MYB, TROAP
Genes involved in NO signaling pathway	CAMK1, DLG4, GRIN2D, NOS1, PPP3CA, PRKAR1B, PRKCA
Genes involved in superoxide release	ALOX12, DUOX1, DUOX2, NOX5, PRG3
Genes with oxidoreductase activity	ALOX12, CYBA, DUOX1, DUOX2, NOS2A, NOX5, SOD1, SOD2, SOD3
Genes with peroxidase activity	DUOX1, DUOX2
Genes with superoxide dismutase activity	SOD2
Other genes involved in superoxide metabolism	CCS, NCF1, NCF2, PREX1
Anti-apoptosis genes	MPO, MTL5, NME5, PRDX2, RNF7
Genes with antioxidant activity	APOE, MT3, SELS, SOD1, SOD3, SRXN1 (C20orf139)
Genes with glutathione peroxidase activity	GPX1, GPX2, GPX3, GPX4, GPX5, GPX6, LOC493869
Genes with oxidoreductase activity	CAT, EPX, GPX1, GPX2, GPX3, GPX4, GPX5, GPX6, LPO, MPO, MSRA, PRDX2, PRDX6, SOD1, SOD2, SRXN1(C20orf139), TPO, TXNRD2
Genes with peroxidase activity	CYGB, EPX, GPR156, LPO, MPO, PRDX2, PRDX5, PRDX6, TPO, TTN, UNR
Transcription regulators	FOXO1, GPR156, SCRT2, SIRT2, SOD2, UNR
Other genes involved in oxidative stress	ATOX1, DUSP1, GSS, KRT1, MBL2, NUDT1, OXR1, PNKP, PRNP, SCARA3, SEPP1, SGK2
DNA damage signaling	
Apoptosis	ABL1, BRCA1, CIDEA, GADD45A, GADD45G, GML, IHPK3, PCBP4, AIFM1 (PDCD8), PPP1R15A, RAD21, TP53, TP73
Cell cycle arrest	CHEK1, CHEK2, DDIT3 (CHOP), GADD45A, GML, GTSE1, HUS1, MAP2K6, MAPK12, PCBP4, PPP1R15A, RAD17, RAD9A, SESN1, ZAK
Cell cycle checkpoint	ATR, BRCA1, FANCG, NBN (NBS1), RAD1, RBBP8, SMC1A (SMC1L1), TP53
Damaged DNA binding	ANKRD17, BRCA1, DDB1, DMC1, ERCC1, FANCG, FEN1, MPG, MSH2, MSH3, N4BP2, NBN (NBS1), OGG1, PMS2L3 (PMS2L9), PNKP, RAD1, RAD18, RAD51, RAD51L1, REV1 (REV1L), SEMA4A, XPA, XPC, XRCC1, XRCC2, XRCC3
Base-excision repair	APEX1, MBD4, MPG, MUTYH, NTHL1, OGG1, UNG
Double-strand break repair	CIB1, FEN1, XRCC6 (G22P1), XRCC6BP1 (KUB3), MRE11A, NBN (NBS1), PRKDC, RAD21, RAD50
Mismatch Repair	ABL1, ANKRD17, EXO1, MLH1, MLH3, MSH2, MSH3, MUTYH, N4BP2, PMS1, PMS2, PMS2L3 (PMS2L9), TP73, TREX1
Other genes related to DNA repair	APEX2, ATM, ATRX, BTG2, CCNH, CDK7, CRY1, ERCC2 (XPD), GTF2H1, GTF2H2, IGHMBP2, LIG1, MNAT1, PCNA, RPA1, SUMO1
Mitochondria	
Membrane polarization & potential	BAK1, BCL2, BCL2L1, BNIP3, SOD1, TP53, UCP1, UCP2, UCP3
Mitochondrial transport	AIP, BAK1, BCL2, BCL2L1, BNIP3, CPT1B, CPT2, DNAJC19, FXC1 (TIMM10B), GRPEL1, HSP90AA1, HSPD1, IMMP2L, MFN2, MIPEP, MTX2, STARD3, TP53, TSPO, UCP1, UCP2, UCP3
Small molecule transport	SLC25A1, SLC25A10, SLC25A12, SLC25A13, SLC25A14, SLC25A15, SLC25A16, SLC25A17, SLC25A19, SLC25A2, SLC25A20, SLC25A21, SLC25A22, SLC25A23, SLC25A24, SLC25A25, SLC25A27, SLC25A3, SLC25A30, SLC25A31, SLC25A37, SLC25A4, SLC25A5
Targeting proteins to mitochondria	AIP, DNAJC19, FXC1 (TIMM10B), GRPEL1, HSPD1, IMMP2L, MFN2, MIPEP, TSPO
Mitochondrion protein import	AIP, COX10, COX18, DNAJC19, FXC1 (TIMM10B), GRPEL1, HSPD1, MIPEP, SH3GLB1
Outer membrane translocation	TOMM20, TOMM22, TOMM34, TOMM40, TOMM40L, TOMM70A
Inner membrane translocation	FXC1 (TIMM10B), IMMP1L, IMMP2L, OPA1, TAZ, TIMM10, TIMM17A, TIMM17B, TIMM22, TIMM23, TIMM44, TIMM50, TIMM8A, TIMM8B, TIMM9
Mitochondrial fission & fusion	COX10, COX18, FIS1, MFN1, MFN2, OPA1
Mitochondrial localization	DNM1L, LRPPRC, MFN2, MSTO1, NEFL, OPA1, RHOT1, RHOT2, UXT
Apoptotic genes	AIFM2, BAK1, BBC3, BCL2, BCL2L1, BID, BNIP3, CDKN2A, DNM1L, PMAIP1, SFN, SH3GLB1, SOD2, TP53
Hypoxia signaling	
Response to Hypoxia	ANGPTL4, ARNT2, CREBBP, EP300, HIF1A, MT3, PRKAA1
Response to oxidative stress	CAT, CYGB, GPX1, PIP3-E
Immune response	GPI, IL1A, IL6, IL6ST, NOS2A, NOTCH1, PTX3, RARA
Other genes related to stress response	ADM, EPO, HYOU1, VEGFA
Hemoglobin complex associated genes	CYGB, EPO, HBB, HMOX1, NOS2A, PIP3-E
Peroxidase	CAT, CYGB, GPX1, PIP3-E
Other oxidoreductase-related genes	HIF1AN, HMOX1, MT3, NOS2A, PLOD3, TH
Transcription co-factors	CREBBP, DR1, ENO1, EP300, EPAS1, HTATIP, RARA
Transcription factors	ARNT2, BHLHB2, CREBBP, ENO1, EP300, EPAS1, HIF1A, HIF3A, KHSRP, MYBL2, PPARA, RARA
Other transcription factors & regulators	HIF1AN, NOTCH1
Anti-apoptosis	BAX, ANGPTL4, BIRC5, IL1A, MYBL2, PEA15, PRKAA1, VEGFA
Caspase activity	BIRC5, CASP1

Caspase inhibition	CD27 (TNFRSF7)
Anti-apoptosis genes	FAS, TNFRSF10D, TNFRSF18, TNFRSF6B, CD27 (TNFRSF7)
Other apoptosis genes	CD40, LTBR, NGFR, TNFRSF10C, TNFRSF11B, TNFRSF12A, TNFRSF14, TNFRSF1A, TNFRSF1B, TNFRSF21
Inflammatory response	CD40, TNFRSF1A
NF-kB signaling pathway	CD40, EDA2R, LTBR, TNFRSF10A, TNFRSF10B, TNFRSF1A, CD27 (TNFRSF7), TRADD
JNK signaling pathway	EDA2R, TNFRSF19, CD27 (TNFRSF7)
Other TNF receptor superfamily members	TNFRSF11A, TNFRSF13B, TNFRSF13C, TNFRSF17, TNFRSF19L, TNFRSF4, TNFRSF8
Induction of apoptosis	CASP3, CRADD, FADD, TRADD
Caspases	CASP2, CASP3, CASP8
Anti-apoptosis genes	BAG4, CASP2, TNF
Other apoptosis genes	DFFA, PAK1, TNFRSF1A, TRAF2
Inflammatory response	TNF, TNFRSF1A
NF-kB signaling pathway	CASP8, FADD, TNF, TNFRSF1A, TRADD
JNK signaling pathway	MAP2K4, MAPK8, PAK1
Transcription regulators	JUN, PARP1, RB1, TNF, TNFRSF1A
TNFR1 signaling pathway	ARHGDI1B, CAD, HRB, LMNA, LMNB1, LMNB2, MADD, MAP3K1, MAP3K7, PAK2, PRKDC, SPTAN1
Induction of apoptosis	IKBK1, LTA, TRAF3
Anti-apoptosis genes	NFKB1, TNFAIP3
Other apoptosis genes	NFKBIA, TNFRSF1B, TRAF1, TRAF2
Inflammatory response	NFKB1
NF-kB signaling pathway	CHUK, IKKB1, IKBK1, NFKBIA, TNFAIP3
Transcription regulators	IKBK1, IKBK1, NFKB1, NFKBIA
TNFR2 signaling pathway	DUSP1, HRB, IKBK1, MAP3K1, MAP3K14, TANK

Supplement T2 – Lists of oxidative-response genes in the pathways shown in Supplement T1

Unigene	Symbol	Description	Unigene	Symbol	Description
Hs.470316	ACVR1	Activin A receptor, type I	Hs.166186	CHRD	Chordin
Hs.470174	ACVR2A	Activin A receptor, type IIA	Hs.172928	COL1A1	Collagen, type I, alpha 1
Hs.591026	ACVRL1	Activin A receptor type II-like 1	Hs.489142	COL1A2	Collagen, type I, alpha 2
Hs.112432	AMH	Anti-Mullerian hormone	Hs.443625	COL3A1	Collagen, type III, alpha 1
Hs.659889	AMHR2	Anti-Mullerian hormone receptor, type II	Hs.304682	CST3	Cystatin C
Hs.533336	BAMBI	BMP and activin membrane-bound inhibitor homolog (<i>Xenopus laevis</i>)	Hs.419	DLX2	Distal-less homeobox 2
			Hs.76753	ENG	Endoglin
Hs.654541	BGLAP	Bone gamma-carboxyglutamate (gla) protein	Hs.656395	EVI1	Ecotropic viral integration site 1
Hs.1274	BMP1	Bone morphogenetic protein 1	Hs.709461	FKBP1B	FK506 binding protein 1B, 12.6 kDa
Hs.73853	BMP2	Bone morphogenetic protein 2	Hs.25647	FOS	V-fos FBJ murine osteosarcoma viral oncogene homolog
Hs.387411	BMP3	Bone morphogenetic protein 3			
Hs.68879	BMP4	Bone morphogenetic protein 4	Hs.9914	FST	Follistatin
Hs.296648	BMP5	Bone morphogenetic protein 5	Hs.279463	GDF2	Growth differentiation factor 2
Hs.285671	BMP6	Bone morphogenetic protein 6	Hs.86232	GDF3	Growth differentiation factor 3
Hs.473163	BMP7	Bone morphogenetic protein 7	Hs.1573	GDF5	Growth differentiation factor 5
Hs.660998	BMPER	BMP binding endothelial regulator	Hs.492277	GDF6	Growth differentiation factor 6
Hs.524477	BMPR1A	Bone morphogenetic protein receptor, type IA	Hs.447688	GDF7	Growth differentiation factor 7
Hs.598475	BMPR1B	Bone morphogenetic protein receptor, type IB	Hs.440438	GSC	Goosecoid homeobox
Hs.471119	BMPR2	Bone morphogenetic protein receptor, type II (serine/threonine kinase)	Hs.632033	HIPK2	Homeodomain interacting protein kinase 2
			Hs.504609	ID1	Inhibitor of DNA binding 1, dominant negative helix-loop-helix protein
Hs.437705	CDC25A	Cell division cycle 25 homolog A (<i>S. pombe</i>)			
Hs.370771	CDKN1A	Cyclin-dependent kinase inhibitor 1A (p21, Cip1)	Hs.180919	ID2	Inhibitor of DNA binding 2, dominant negative helix-loop-helix protein
Hs.72901	CDKN2B	Cyclin-dependent kinase inhibitor 2B (p15, inhibits CDK4)	Hs.160562	IGF1	Insulin-like growth factor 1 (somatomedin C)
Hs.248204	CER1	Cerberus 1, cysteine knot superfamily, homolog (<i>Xenopus laevis</i>)	Hs.450230	IGFBP3	Insulin-like growth factor binding protein 3
			Hs.654458	IL6	Interleukin 6 (interferon, beta 2)

Hs.407506	INHA	Inhibin, alpha	N/A	HGDC	Human Genomic DNA Contamination
Hs.583348	INHBA	Inhibin, beta A	Hs.431048	ABL1	C-abl oncogene 1, receptor tyrosine kinase
Hs.1735	INHBB	Inhibin, beta B	Hs.601206	ANKRD17	Ankyrin repeat domain 17
Hs.536663	ITGB5	Integrin, beta 5	Hs.73722	APEX1	APEX nuclease (multifunctional DNA repair enzyme) 1
Hs.654470	ITGB7	Integrin, beta 7	Hs.367437	ATM	Ataxia telangiectasia mutated
Hs.714791	JUN	Jun oncogene	Hs.271791	ATR	Ataxia telangiectasia and Rad3 related
Hs.25292	JUNB	Jun B proto-oncogene	Hs.533526	ATRX	Alpha thalassemia/mental retardation syndrome X-linked (RAD54 homolog, <i>S. cerevisiae</i>)
Hs.656214	LEFTY1	Left-right determination factor 1	Hs.194143	BRCA1	Breast cancer 1, early onset
Hs.713533	LTBP1	Latent transforming growth factor beta binding protein 1	Hs.519162	BTG2	BTG family, member 2
Hs.512776	LTBP2	Latent transforming growth factor beta binding protein 2	Hs.292524	CCNH	Cyclin H
Hs.466766	LTBP4	Latent transforming growth factor beta binding protein 4	Hs.184298	CDK7	Cyclin-dependent kinase 7
Hs.202453	MYC	V-myc myelocytomatosis viral oncogene homolog (avian)	Hs.24529	CHEK1	CHK1 checkpoint homolog (<i>S. pombe</i>)
Hs.654502	NBL1	Neuroblastoma, suppression of tumorigenicity 1	Hs.291363	CHEK2	CHK2 checkpoint homolog (<i>S. pombe</i>)
Hs.370414	NODAL	Nodal homolog (mouse)	Hs.135471	CIB1	Calcium and integrin binding 1 (calmyrin)
Hs.248201	NOG	Noggin	Hs.249129	CIDEA	Cell death-inducing DFFA-like effector a
Hs.268490	NR0B1	Nuclear receptor subfamily 0, group B, member 1	Hs.151573	CRY1	Cryptochrome 1 (photolyase-like)
Hs.1976	PDGFB	Platelet-derived growth factor beta polypeptide (simian sarcoma viral (v-sis) oncogene homolog)	Hs.290758	DDB1	Damage-specific DNA binding protein 1, 127kDa
Hs.77274	PLAU	Plasminogen activator, urokinase	Hs.505777	DDIT3	DNA-damage-inducible transcript 3
Hs.149261	RUNX1	Runt-related transcription factor 1	Hs.339396	DMC1	DMC1 dosage suppressor of mck1 homolog, meiosis-specific homologous recombination (yeast)
Hs.414795	SERPINE1	Serpin peptidase inhibitor, clade E (nexin, plasminogen activator inhibitor type 1), member 1	Hs.435981	ERCC1	Excision repair cross-complementing rodent repair deficiency, complementation group 1 (includes overlapping antisense sequence)
Hs.604588	SMAD1	SMAD family member 1	Hs.487294	ERCC2	Excision repair cross-complementing rodent repair deficiency, complementation group 2
Hs.12253	SMAD2	SMAD family member 2	Hs.498248	EXO1	Exonuclease 1
Hs.714621	SMAD3	SMAD family member 3	Hs.591084	FANCG	Fanconi anemia, complementation group G
Hs.75862	SMAD4	SMAD family member 4	Hs.409065	FEN1	Flap structure-specific endonuclease 1
Hs.167700	SMAD5	SMAD family member 5	Hs.292493	XRCC6	X-ray repair complementing defective repair in Chinese hamster cells 6
Hs.189329	SMURF1	SMAD specific E3 ubiquitin protein ligase 1	Hs.80409	GADD45A	Growth arrest and DNA-damage-inducible, alpha
Hs.643910	SOX4	SRY (sex determining region Y)-box 4	Hs.9701	GADD45G	Growth arrest and DNA-damage-inducible, gamma
Hs.642990	STAT1	Signal transducer and activator of transcription 1, 91kDa	Hs.661218	GML	Glycosylphosphatidylinositol anchored molecule like protein
Hs.645227	TGFB1	Transforming growth factor, beta 1	Hs.577202	GTF2H1	General transcription factor IIH, polypeptide 1, 62kDa
Hs.513530	TGFB11	Transforming growth factor beta 1 induced transcript 1	Hs.191356	GTF2H2	General transcription factor IIH, polypeptide 2, 44kDa
Hs.507916	TSC22D1	TSC22 domain family, member 1	Hs.386189	GTSE1	G-2 and S-phase expressed 1
Hs.133379	TGFB2	Transforming growth factor, beta 2	Hs.152983	HUS1	HUS1 checkpoint homolog (<i>S. pombe</i>)
Hs.592317	TGFB3	Transforming growth factor, beta 3	Hs.503048	IGHMBP2	Immunoglobulin mu binding protein 2
Hs.369397	TGFB1	Transforming growth factor, beta-induced, 68kDa	Hs.17253	IP6K3	Inositol hexakisphosphate kinase 3
Hs.494622	TGFBR1	Transforming growth factor, beta receptor 1	Hs.61188	XRCC6BP1	XRCC6 binding protein 1
Hs.604277	TGFBR2	Transforming growth factor, beta receptor II (70/80kDa)	Hs.1770	LIG1	Ligase I, DNA, ATP-dependent
Hs.482390	TGFBR3	Transforming growth factor, beta receptor III	Hs.463978	MAP2K6	Mitogen-activated protein kinase kinase 6
Hs.446350	TGFBRAP1	Transforming growth factor, beta receptor associated protein 1	Hs.432642	MAPK12	Mitogen-activated protein kinase 12
Hs.373550	TGIF1	TGFB-induced factor homeobox 1	Hs.35947	MBD4	Methyl-CpG binding domain protein 4
Hs.534255	B2M	Beta-2-microglobulin	Hs.195364	MLH1	MutL homolog 1, colon cancer, non-polyposis type 2 (<i>E. coli</i>)
Hs.412707	HPRT1	Hypoxanthine phosphoribosyltransferase 1	Hs.436650	MLH3	MutL homolog 3 (<i>E. coli</i>)
Hs.523185	RPL13A	Ribosomal protein L13a	Hs.509523	MNAT1	Menage-a-trois homolog 1, cyclin H assembly factor (<i>Xenopus laevis</i>)
Hs.592355	GAPDH	Glyceraldehyde-3-phosphate dehydrogenase			
Hs.520640	ACTB	Actin, beta			

Hs.459596	MPG	N-methylpurine-DNA glycosylase	Hs.631709	RAD51	RAD51 homolog (RecA homolog, <i>E. coli</i>)
Hs.192649	MRE11A	MRE11 meiotic recombination 11 homolog A (<i>S. cerevisiae</i>)	Hs.172587	RAD51L1	RAD51-like 1 (<i>S. cerevisiae</i>)
Hs.597656	MSH2	MutS homolog 2, colon cancer, non-polyposis type 1 (<i>E. coli</i>)	Hs.655354	RAD9A	RAD9 homolog A (<i>S. pombe</i>)
Hs.280987	MSH3	MutS homolog 3 (<i>E. coli</i>)	Hs.546282	RBBP8	Retinoblastoma binding protein 8
Hs.271353	MUTYH	MutY homolog (<i>E. coli</i>)	Hs.443077	REV1	REV1 homolog (<i>S. cerevisiae</i>)
Hs.391463	N4BP2	Nedd4 binding protein 2	Hs.461925	RPA1	Replication protein A1, 70 kDa
Hs.492208	NBN	Nibrin	Hs.408846	SEMA4A	Sema domain, immunoglobulin domain (Ig), transmembrane domain (TM) and short cytoplasmic domain, (semaphorin) 4A
Hs.66196	NTHL1	Nth endonuclease III-like 1 (<i>E. coli</i>)	Hs.591336	SESN1	Sestrin 1
Hs.380271	OGG1	8-Oxoguanine DNA glycosylase	Hs.211602	SMC1A	Structural maintenance of chromosomes 1A
Hs.20930	PCBP4	Poly(rC) binding protein 4	Hs.81424	SUMO1	SMT3 suppressor of mif two 3 homolog 1 (<i>S. cerevisiae</i>)
Hs.147433	PCNA	Proliferating cell nuclear antigen	Hs.654481	TP53	Tumor protein p53
Hs.424932	AIFM1	Apoptosis-inducing factor, mitochondrion-associated, 1	Hs.697294	TP73	Tumor protein p73
Hs.111749	PMS1	PMS1 postmeiotic segregation increased 1 (<i>S. cerevisiae</i>)	Hs.707026	TREX1	Three prime repair exonuclease 1
Hs.632637	PMS2	PMS2 postmeiotic segregation increased 2 (<i>S. cerevisiae</i>)	Hs.191334	UNG	Uracil-DNA glycosylase
Hs.225784	PMS2L3	Postmeiotic segregation increased 2-like 3	Hs.654364	XPA	<i>Xeroderma pigmentosum</i> , complementation group A
Hs.78016	PNKP	Polynucleotide kinase 3'-phosphatase	Hs.475538	XPC	<i>Xeroderma pigmentosum</i> , complementation group C
Hs.631593	PPP1R15A	Protein phosphatase 1, regulatory (inhibitor) subunit 15A	Hs.98493	XRCC1	X-ray repair complementing defective repair in Chinese hamster cells 1
Hs.491682	PRKDC	Protein kinase, DNA-activated, catalytic polypeptide	Hs.647093	XRCC2	X-ray repair complementing defective repair in Chinese hamster cells 2
Hs.531879	RAD1	RAD1 homolog (<i>S. pombe</i>)	Hs.592325	XRCC3	X-ray repair complementing defective repair in Chinese hamster cells 3
Hs.16184	RAD17	RAD17 homolog (<i>S. pombe</i>)	Hs.444451	ZAK	Sterile alpha motif and leucine zipper containing kinase AZK
Hs.375684	RAD18	RAD18 homolog (<i>S. cerevisiae</i>)			
Hs.81848	RAD21	RAD21 homolog (<i>S. pombe</i>)			
Hs.655835	RAD50	RAD50 homolog (<i>S. cerevisiae</i>)			

Importance of CDK7 for G1 Re-Entry into the Mammalian Cell Cycle and Identification of New Downstream Networks Using a Computational Method

Hideko Sone^{*,1,2,§}, Tomokazu Fukuda^{3,§}, Hiroyoshi Toyoshiba^{1,§}, Takeharu Yamanaka¹, Fred Parham¹ and Christopher J. Portier¹

¹Laboratory of Computational Biology and Risk Analysis, National Institute of Environmental Health Sciences, 111 T.W. Alexander Drive, Research Triangle Park, NC 27709, USA

²Health Effects Team, National Institute for Environmental Studies, 16-2 Onogawa, Tsukuba 305-8506, Japan

³Laboratory of Animal breeding and Genetics, Graduate school of Agricultural Science, Tohoku University, Tsutsumidori-amamiyamachi 1-1 Aoba-ku, Sendai 981-8555, Japan

Abstract: Many of the key molecules in cell cycle progression (e.g. pRB, cyclin complexes) and their basic interactions are oncogene or tumor suppressor genes, which are well characterized in the clinical and experimental analysis. However, there are still unknown mechanisms for the cell cycle regulation, which is critical step for the progression of the cancer development. Especially it is not fully understood how the cells move to G1 phase from quiescent G0 phase in the mammalian cells. To find out the new gene networks associated with the two transition of the mammalian cell cycle (G0 to G1 and G1 to S phase), we analyzed the linkages between 39 representative oncogene or tumor suppressor genes, which related to the cell cycle regulation, with gene expression sets obtained from the publicly opened microarray data for mouse embryonic fibroblasts that synchronized by the serum starvation or hydroxyurea treatment. Analyses with a qualitative algorithm based on Bayesian networks that assume a log-linear relationship between genes have applied, and newly found networks were validated. Results highlighted the importance of two master genes, *Cdk7* and *Cdkna2* for the re-entry to G1 from G0, and suggested a new network connection from *Cdk7* to downstream molecules, including the *EGF* receptor and *N-myc*. Introduction of a recombinant *Cdk7* with retrovirus decreased endogenous EGFR and N-myc protein levels. The results supported the computational prediction of the *Cdk7* network. Taken together, these result showed the existence of new regulating pathway from *Cdk7* to *Egfr* and *N-myc*, suggesting this analytical approach provides an assessment of regulatory networks in complex mammalian cells, and the process of the carcinogenesis.

Keywords: Gene network, cell cycle, Cdk7, mammalian, Bayesian theory.

INTRODUCTION

Cell division and tissue growth represent two of the most fundamental biological processes and play essential roles in development, aging, cancer [1, 2], and many other diverse events. Although gene transcripts have been comprehensively catalogued in yeast, much work remains to be done in higher organisms. Especially, for tumor progression, the gene networks underlying the regulation of the cell cycle are not well understood in cancer cells or the initiated precancerous cells. Several groups have utilized microarrays to perform serial analyses of gene expression during cellular replication in normal or cancer human and mouse cell lines [3-6]. These microarray data have been analyzed using clustering approaches such as hierarchical clustering and k-means to identify stage-specific or co-regulated genes through each phase of the cell cycle. However, these methodologies can

only identify genes with expression levels that correlate over time, and the network dynamics of the cell cycle is not yet fully understood.

Integrated and networked functions in mammalian cells can be identified and quantified through the use of a computational model. Efforts to systematically define specific gene network structures to further understand the functions and dynamics of each gene and its protein products have lead to a new generation of *in silico* analysis tools that use diagrams to depict the logical relationships between genes [7-9]. To infer unknown gene networks from microarray gene expression data, the methods adopted need to incorporate the two different aspects of Bayesian models and associated validation tools. The application of these biostatistical methods has the potential to elucidate unknown mechanisms underlying the key regulatory systems of mammalian cells [10-12].

The regulatory mechanisms for the G0 quiescent stage of the cell cycle remain largely unknown. For the efficient progression from the G0 to G1 phase, the protein level of the p27/kip1 is known to have a important role in T cell from *in vitro* study and a knockout mouse study [13, 14]. In the normal cells, the protein level of p27 is high during G0 phase

*Address correspondence to this author at the Research Center for Environmental Risk, National Institute for Environmental Studies, 16-2 Onogawa, Tsukuba 305-8506, Japan; Tel: +81.298.50.2464; Fax: +81.298.50.2546; E-mail: hsone@nies.go.jp

§These authors equally contributed to this work.

but decreases rapidly on the entry to G1 [14, 15]. The degradation of p27 is controlled by an SCF complex, which involves SKP2 [16, 17]. Although these findings for G0-G1 regulation have had a significant impact, it is not clear whether these mechanisms can be applied to the all type of cells and tissues. For cancer therapeutics, the G0-G1 transition of the cell cycle has been a strong target to prevent tumor growth and progression [18-20].

In our current study, we employed the gene datasets from the publicly opened microarray data for the mouse fibroblasts, which synchronized with the serum starvation and hydroxyurea, which are the study of the transition from a quiescent state into the cell cycle in mouse embryonic fibroblast (MEF) cells reported by Ishida *et al.* [4]. In order to elucidate new gene networks related to the progression of the cell cycle, the gene expression datasets were analyzed using a series of approaches in which putative network structures are elucidated using Bayesian networks. These approaches involve a likelihood-based selection algorithm to qualitatively infer the identity of the network structure [21] and a quantitative algorithm involving a Markov chain Monte Carlo (MCMC) method [22, 23] is then used to quantify the structure. The identified interactions between genes that are based upon these predicted gene networks were then validated using a retrovirus expression system.

MATERIALS AND METHODS

Microarray Data Sets

Previously published mouse embryonic fibroblast (MEF) cell microarray datasets were used in our analyses [4].

Briefly, the cells were synchronized by either serum starvation or hydroxyurea treatment. We used the data sets obtained from the serum starved cells for the analysis of re-entry into G1 from G0 (0, 6, 12, 15, 18, 21, 24 hours after serum starvation), and those from the hydroxyurea exposed fibroblasts for the G1-S analysis (0, 3, 6, 9, 12, 15, 18 hours after the treatment). The detailed methods used to obtain these microarray data have been previously described [4].

Selection of the Subset Database

The original gene expression data, comprising about 6437 genes, were screened for genes that showed at least a 2.0-fold change (up- or down-regulation) using GenMAPP [24]. The distribution and frequency of the fold changes (relative to the time 0) at each time point were analyzed by MAPFinder 1.0 beta, an accessory tool of GenMAPP, to identify the optimal biological maps. From this collection of maps, we selected those related to cell cycle processes that had a “z” score greater than 1.95 (the z score represents the difference between the observed number of genes meeting the criteria and the expected number of genes meeting the criteria in each map based on gene ontology). As detailed in Table 1, 10 maps were selected based on gene ontology (denoted MAPP) and the relationship to the cell cycle. A subset of 39 genes was chosen from among the MAPP maps selected (Table 2). The abbreviated names of the genes that were analyzed in this report are presented according to the displays listed in GenMAPP.

Mathematical Models

We applied the expression-associated network modeling method previously developed by Yamanaka *et al.* [21] to the

Table 1. List of Maps with More than 1.95 Z Score Selected from Maps Analyzed by MAPFinder. Maps are the Database from Mouse Biological Processes that are Contain in GenMAPP

MAPP Name	A	B	C	D	E	R	z Score	Time Point
Mm_cell cycle	4	15	104	26.7	14.4	95	2.014	18h
	4	15	104	26.7	14.4	87	2.211	21h
Mm_cell cycle arrest	2	2	11	100	18.2	92	4.175	12h
	2	2	11	100	18.2	92	4.175	15h
	2	2	11	100	18.2	109	3.795	18h
	2	2	11	100	18.2	118	3.626	21h
	2	2	11	100	18.2	121	4.335	24h
Mm_cell cycle control	15	48	124	31.2	38.7	132	3.205	12h
	9	48	124	18.8	38.7	87	2.102	21h
Mm_cell growth and or maintenance	17	55	153	30.9	35.9	132	3.357	12h
Mm_cell growth	3	7	16	42.9	43.8	118	2.317	21h
Mm_cell proliferation	3	4	28	75	14.3	95	4.177	18h
Mm_G1 S transition of	1	1	5	100	20	101	2.771	6h
Mitotic cell cycle								
Mm_mitosis	2	6	23	33.3	26.1	87	1.95	21h
Mm_mitotic cell cycle	1	1	7	100	14.3	101	2.771	6h
Mm_M phase of mitotic cell cycle	2	6	23	33.3	26.1	87	1.95	21h

A, the number of genes meeting the criterion in this specific MAPP; B, the total number of genes measured in this specific MAPP; C, Number on MAPP; D, Percent Changed; E, Percent present; N, the total number of genes measured (= 894), R, the total number of distinct genes meeting the criterion. Criteria were set at > 2.0 or < 0.5 of the expression ratio. Each time point means a sampling time after serum starvation. Z Score = $(A - B * R / N) / \sqrt{(B / (R * N) * (1 - R / N) * (1 - B / (N - 1)))}$.

Table 2. List of Name Abbreviations and Description of the Genes Analyzed in this Study

Gene Name	Description
<i>Abl1</i>	Mouse c-abl gene exon 1 of type II
<i>Ccnal</i>	Mouse mRNA for cyclin A1
<i>Ccn2</i>	Mouse mRNA for cyclin A2
<i>Ccnb2</i>	Mouse mRNA for cyclin B2
<i>Ccne1</i>	Mouse mRNA for cyclin E
<i>Crkl</i>	Mouse mRNA for Crkl protein
<i>Csf1r</i>	Mouse c-fms proto-oncogene
<i>E2f5</i>	Mouse mRNA for E2F-5 protein
<i>Egfr</i>	Mouse (BALB/c) Epidermal Growth Factor Receptor mRNA
<i>Elk1</i>	Mouse mRNA for elk 1 protein
<i>Elk4</i>	Mouse sap1A mRNA
<i>Ets1</i>	Mouse ets-1 mRNA
<i>Etv6</i>	Mouse mRNA for TEL protein
<i>Fgf3</i>	Mouse int-2 gene
<i>Fgf</i>	Mouse mRNA for new member of PDGF/VEGF family of growth factors
<i>Fos</i>	Mouse c-fos oncogene
<i>Fosb</i>	Mouse fosB mRNA
<i>Il1a</i>	Mouse mRNA for interleukin-1
<i>Lmyc1</i>	Mouse L-myc gene
<i>Mybl2</i>	Mouse B-myb mRNA
<i>Myc</i>	Mouse normal c-myc gene
<i>Nmyc1</i>	Mouse N-myc gene
<i>Nras</i>	Mouse mRNA for N-ras protein (exons 1 - 6 part.)
<i>Pdgfb</i>	Mouse platelet-derived growth factor B chain (c-sis) gene
<i>Pgf</i>	Mouse mRNA for placenta growth factor
<i>Ptn</i>	Mouse mRNA for OSF-1
<i>Ret</i>	Mouse mRNA for ret proto-oncogene
<i>Tfdp1</i>	Mouse mRNA for DRITF-polypeptide-1 (DP-1)
<i>Tgfb2</i>	Mouse mRNA for transforming growth factor-beta2
<i>Thra</i>	Mouse c-erbA-alpha mRNA for thyroid hormone receptor
<i>Tlm</i>	Mouse tlm oncogene for tlm protein
<i>Cdkn2a</i>	Mouse CDK4 and CDK6 inhibitor protein (p16ink4a)
<i>Cdkn2d</i>	Mouse p19 protein mRNA, complete cds
<i>E2F1</i>	Mouse E2F1 mRNA, complete cds
<i>p53</i>	Mouse mRNA for cellular tumour antigen p53
<i>mdm2</i>	Mouse mdm2 mRNA for mdm2 protein
<i>Cdk7</i>	Mouse mRNA for protein kinase crk4
<i>Rbl1</i>	Mouse p107 (p107) mRNA, complete cds
<i>Rbl2</i>	Mouse retinoblastoma-related protein Rb2/p130

fold-change data from the gene-expression data sets. This method falls under the general area of Bayesian networks, with a likelihood-based selection algorithm used to identify the most promising networks. In general, if X_1, X_2, \dots, X_p represents the data obtained for p genes, N denotes a network, and θ denotes parameters in that network, with the likelihood given by:

$$f_{X|N,\theta}(X_1, X_2, \dots, X_p | N, \theta) = \prod_{j=1}^p f_{X_j|N,\theta_j}(X_j | pa(X_j), N, \theta_j) \quad (1)$$

A. The choice of the best network would be the one with the largest value of the posterior density at the chosen network topology; that is

$$\text{find } \hat{N} = \arg \max_N f_{N|D}(N | D) \quad (2)$$

$$\text{where } f_{N|D}(N | D) \propto f_N(N) \cdot f_{D|N}(D | N) \quad (3)$$

B. The Bayesian network used in this analysis had the following assumptions:

$$\text{i) } f_N(N) \Rightarrow \text{uniform distribution} \quad (4)$$

$$\text{ii) } f_{D|\theta,N}(D | \theta, N) = \prod_{j=1}^p \left\{ \prod_{i=1}^n f_{X_{ji}|N,\theta_j}(X_{ji} | pa(X_{ji}), N, \theta_j) \right\} \quad (5)$$

$$\text{iii) } f_{\theta|N}(\theta | N) = \prod_{j=1}^p f_{\theta_j|N}(\theta_j | N) \quad (6)$$

where $pa(X_{ji})$ is the collection of genes that link to the j^{th} gene in the network (a pathway).

with these assumptions,

$$\begin{aligned} &\log f_{N|D}(N | D) \\ &\propto \sum_{j=1}^p \log \int \left\{ \prod_{i=1}^n f_{X_{ji}|N,\theta_j}(X_{ji} | pa(X_{ji}), N, \theta_j) \right\} \cdot f(\theta_j | N) d\theta_j \end{aligned} \quad (7)$$

Thus, it is possible to focus on each gene rather than the whole network and still obtain a global optimum. To quantify rates in the gene-expression network, we used the Bayesian methods developed by Toyoshiba *et al.* [22, 23]. Supposing that X_i ($i=1,2,3\dots p$) represents the natural log of the relative ratio, the functional relationships between the genes could be characterized using the log-linear model below:

$$E(X_i | Pa(X_i), \beta_{i*}) = e^{\sum_{j=1}^p I_{ji} \beta_{ji} X_j} \quad (8)$$

where I_{ji} is an indicator function (-1, 0, 1) characterizing the effect from G_j to G_i , T represents a matrix having I_{ij} as the (i,j) element, and $\beta_{i*} = [\beta_{i1}, \beta_{i2}, \beta_{i3}, \beta_{i4}, \dots, \beta_{ip}]$ is the vector in which each β_{ji} is the magnitude by which one unit of gene X_j will affect the expression levels of gene X_i . Thus, if I_{ji} is not equal to 0, $Pa(X_i)$ contains X_j .

If $f(X_i | T, \theta)$ is defined as the distribution of gene expression in the given model, then the likelihood is written as

$$f_{X|T,\theta}(X_1, X_2, \dots, X_p | T, \theta) = \prod_{j=1}^p f_{X_j|T,Pa(X_j),\theta_j}(X_j | T, Pa(X_j), \theta_j) \quad (9)$$

where θ represents the parameter vector in the model.

By Bayes' theorem, the prior distribution is given by

$$f_{\theta|X,T}(\theta|X,T) \sim f_{X|T,\theta}(X_1, X_2, \dots, X_p|T, \theta) \cdot f_{\theta}(\theta) \quad (10)$$

The posterior distributions $f_{\theta|X,T}$ were evaluated using the MCMC method. In our analyses, $f_{X|T,\theta}$ was assumed to be normal, with a mean defined by equation (8) and a random variance whose prior distribution was assumed to be uniform with 0 as the lower bound and twice the maximum STD for each gene distribution. The prior distribution for θ and f_{θ} was assumed to be lognormal with a mean of 0 and a variance of 1.0

The MCMC analysis was applied as described in [23] and [22]. A typical MCMC run was 100,000 samples with the first 20% of the samples discarded to "burn in" the algorithm. Some runs were much longer depending on convergence and stabilization of the resulting posterior distributions.

The model described in this section is an analysis tool and is not intended to characterize the mechanisms by which the different genes are linked. Instead, it is intended to find the most prominent linkages between cells to provide hypotheses that can be further explored and later modeled mechanistically.

Visualization of Gene Networks and Clustering Analysis

We used a MATLAB script newly developed by Parham *et al.* (unpublished data) to generate transcriptional regulatory networks using MATLAB version 6.5 (The MathWorks, Inc., Natick, MA).

Establishment of Mouse *CDK7* Recombinant Retrovirus

A full length cDNA fragment of mouse cyclin-dependent kinase (*Cdk7*) (NIH Mammalian Gene bank accession number: NMV009874) was obtained by RT-PCR from the total RNA extracts of 13.5 day mouse embryo using a previously described method [25]. A hemagglutinin (HA) protein tag sequence was then introduced at the carboxyl terminus of this mouse *Cdk7* cDNA using a tailed PCR method. The *Cdk7* cDNA was next subcloned into the EcoRV site of pBluescript SKII+ (Stratagene, La Jolla, CA) by blunt end ligation, and the resulting constructs were validated using a cycle sequencing reaction in an ABI 310 genetic analyzer (Applied Biosystems, Foster City, CA). The subcloned *Cdk7* cDNA fragment was then transferred into the multiple cloning site of an LXIN retrovirus vector (Clontech, Mountain View, CA). Both empty LXIN vector and LXIN vector harboring the mouse *Cdk7* cDNA were introduced into PT67 retrovirus packaging cells (Clontech) using Fugene6 (Roche, Basel, Switzerland). Infected cells were then selected with 1mg/ml G418 (Invitrogen, Carlsbad, CA) in the growth media for one week.

Measurement of the Retrovirus Titers in the Producer Cells

Conditioned medium from the producer cells was diluted 1:10 and 1:50 with DMEM containing 10% calf serum, and then used for the infection of NIH3T3 cells to measure the titer of the synthesized retrovirus. NIH3T3 cells were grown

in media with diluted retroviruses for two days under the same conditions that are described below for mouse embryonic fibroblasts. The infected NIH3T3 cells were diluted 1:100 and 1:1000, and then selected with 1mg/ml G418 for one week. Retrovirus titers of the original conditioned medium were calculated based on the number of colonies demonstrating G418 resistance.

Preparation of MEF Cells that Expresses the Recombinant Mouse *CDK7*

Mouse embryonic fibroblasts (MEF) were prepared using a previously described method [25]. Second passage primary fibroblasts at a 70% confluency were infected with conditioned medium containing PT67 producer cells at a 1:2 dilution 1:2 with basal MEF medium for 2 days in the presence of 1 μ g/ml polybrene (Sigma-Aldrich, St. Louis, MO). When the infected MEF cells reached confluence, they were diluted 1:5 as above and selected with 200 μ g/ml G418 for one week. Control experiments confirmed that non-infected MEF cells did not survive in the presence of 200 μ g/ml G418 (data not shown). Infected cells selected with G418 were subjected to lysis and protein extraction for western blot analyses.

Western Blot Analyses of MEF Cells Exogenously Expressing Mouse *CDK7*

Total proteins were isolated from MEF cells infected with either control or *Cdk7* recombinant retrovirus using a standard methodology [25]. Heat-denatured proteins were separated by 10% SDS-PAGE and the proteins in the gel were transferred to polyvinylidene difluoride (PVDF) membranes (Immobilon P, Millipore, Billerica, MA). After blocking with 1% non-fat dry milk-Tris buffered saline and 0.1% Tween 20 (TBST), the membranes were probed with anti-HA (High affinity HA 3F10, 1:5,000 dilution, Roche), anti- α -CDK7 (sc-723, 1:5,000 dilution, Santa Cruz, CA), anti-EGFR (kindly provided by Dr. DiAugustine, RP) and anti-N-MYC1 (sc-791, 1:1,000 dilution, Santa Cruz, CA) and anti-c-FOS (sc-52, 1:1,000 dilution, Santa Cruz, CA) antibodies. Blots were then incubated with horseradish peroxidase (HRP)-conjugated rabbit anti-rat IgG (A5795, 1:5,000 dilution, Roche) or donkey anti-rabbit IgG (1:5,000 dilution, GE Healthcare Bioscience) secondary antibodies, respectively. Immunoreactive proteins were detected by enhanced chemiluminescence (P90720, Millipore). Signal intensities from the western blots were detected with X-ray film and quantified using NIH3T3 image software.

RESULTS

Strategy and Analysis of Gene Network Structures

Our experimental strategy is illustrated in Fig. (1) and consists of three steps: selection of datasets, visualization and analysis by mathematical modeling, and prediction of biological function through the analysis of transcripts. Genome-wide expression data can provide information linking diverse genes and may be useful as a classification tool to identify alterations in biological processes linked to disease. In contrast, carefully designed analyses of a limited gene group associated with a specific biological process can be used to quantify the dynamics of a gene regulatory network. The genes associated with cell cycle regulation are

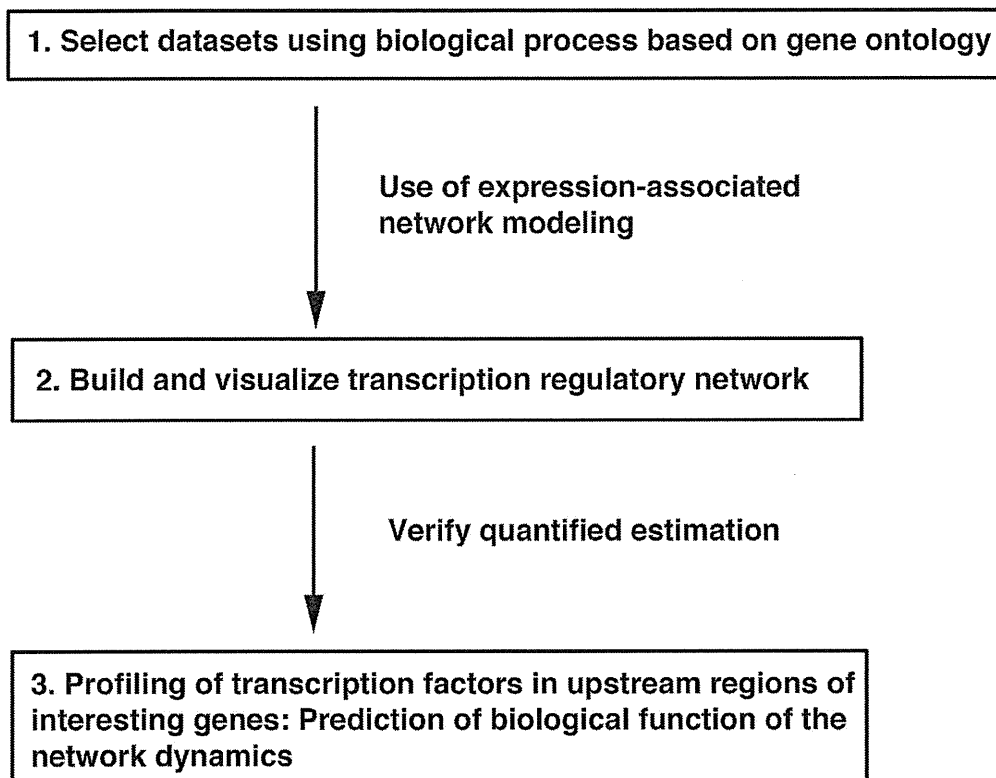


Fig. (1). Strategy used to identify, analyze, and validate regulatory gene networks.

an obvious target for this type of analysis and are the focus of our current study.

The first step in our approach was to select a data subset from a pool of genes associated with various aspects of cell cycle-related processes. The gene choices were based on the gene ontology of the mouse genome using GenMAPP, a computer application designed for the visualization of gene expression data by using maps representing biological pathways. This technique provided a qualitative tool for grouping genes (see Materials and methods). To gather gene expression data associated with the cell cycle, mouse embryo fibroblasts (MEFs) [4] were serum starved or exposed to hydroxyurea to synchronize and control their movement through the cell cycle. At various time points following the release from G0 and cell cycle re-entry, the mRNA expression levels for 6437 genes was measured using a microarray. For 10 cell-cycle related maps (Table 1), 145 genes were measured in the microarray assay. Of these 145 genes, 50 genes met the criteria of at least 2-fold higher or lower levels as shown in Table 1. Since the number of genes analyzed using TAO-gen had to be reduced due to computer processing limitations, 39 out of these 50 genes were finally selected for further analysis based on tissue-specific expression information and their biological significance from published articles after removing overlapping genes.

Two separate maps linking our selected 39 genes to a network were generated using the G0 course data subset (serum starvation) and the G1/S course data subset (hydroxyurea treatment). Although the expression of these genes is dynamic during the cell cycle, the networks were modeled by assuming equilibrium between the genes and by

evaluating those using formal statistical methods that quantified any linkages and assessed their significance. Nodal genes (genes that appeared to be linked to a large number of other genes) were positively identified in the network. In the final verification step, the promoter regions of the genes targeted by each nodal gene were analyzed for common transcriptional factor binding sites. Finally, we discuss the roles of the central nodes and the dynamics of the quantified network in relation to the murine cell cycle.

Identification of a Gene Network Based on Expression Profiles

Representative maps using our 39 gene networks were developed separately for the G0 course (Fig. 2A) and the G1/S course (Fig. 3A). The number of linkages in these two networks is summarized in Table 3. Name abbreviations of the genes analyzed in this paper are shown according to their listing in GenMAPP. These networks were developed using Bayesian networks and a mathematical model allowing each of these mRNAs to connect to any other through direct or indirect transcriptional regulation leading to gene expression changes.

The network from the G0 course data subset in which the cells had been serum starved indicates that the cyclin-dependent kinase inhibitor 2A (*Cdkn2a*) and *Cdk7* are central nodes (Fig. 2B, C), whereas *E2f1*, known to regulate the G0-G1 transition, plays a lesser role. Although the *Cdkn2a* and *Cdk7* gene products and related molecules have been suggested to functions in regulating G1 entry and progression from side supportive data [26, 27], it was not clear until our current findings whether these molecules

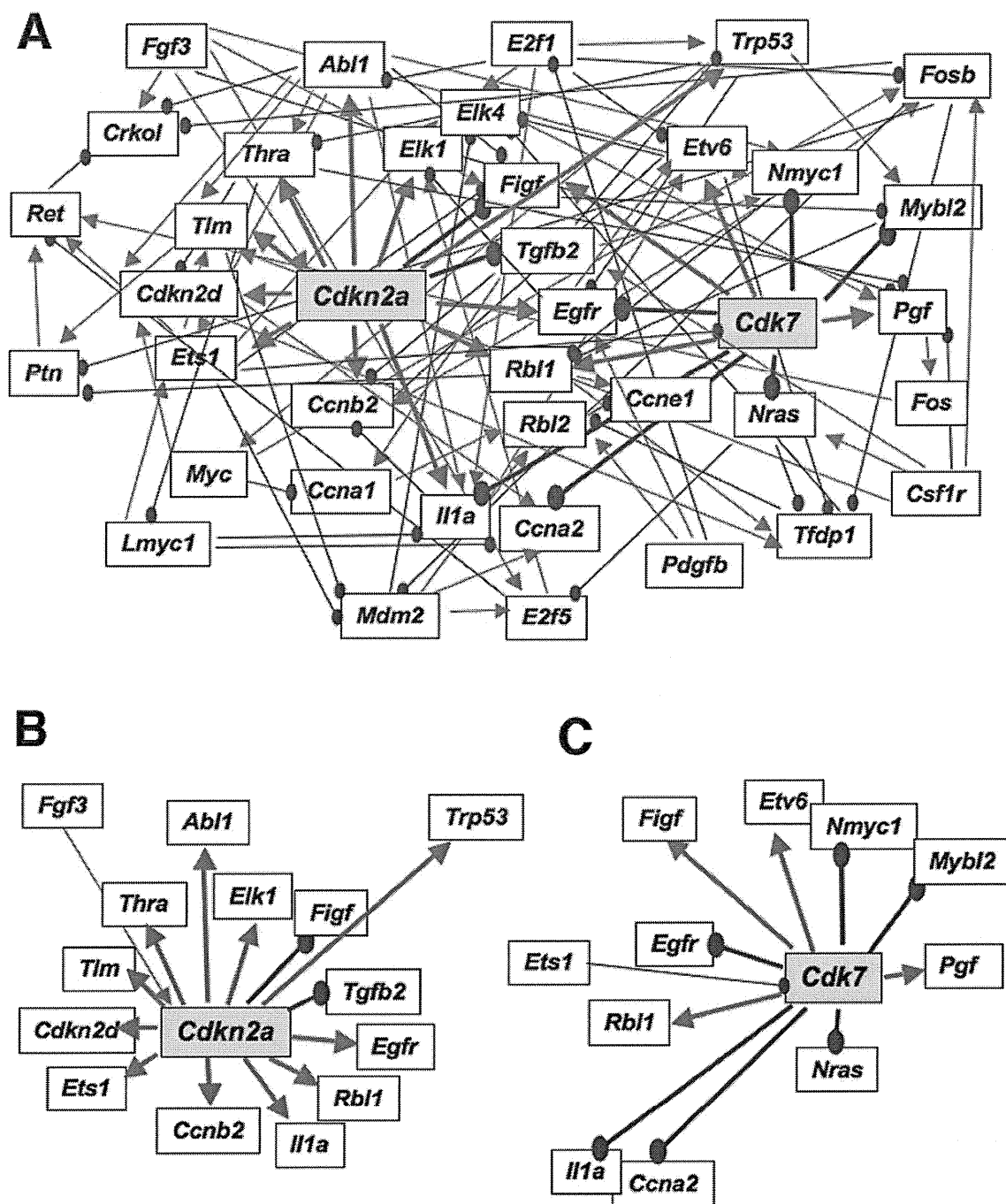


Fig. (2). Representative maps and expression graphs of the transcriptional regulatory networks for selected genes associated with cell-cycle control in MEF cells. Shown are (A) the network identified for the G0 course data and also the isolated linkages associated with nodal genes *Cdkn2a* (B) and *Cdk7* (C). Bold lines indicate linkages from *Cdkn2a* or *Cdk7* as a nodal gene. Red arrows indicate linkages associated with upregulation and blue arrows indicate linkages associated with downregulation for any two genes within the network.

functioned as central nodes in the gene networks. *Cdkn2a* and *Cdk7* were not classified as a G0 cluster via k-means in the first report of these microarray data [4]. CDKs are known to be key components of the core cell cycle machinery and are inhibited by cyclin-dependent protein kinase inhibitors (CKNs). CDK7 and CDKN2A are members of the CDK and CDKN families, respectively. *Cdkn2a* also encodes p16^{INK4a}, a protein that indirectly regulates the activities of both pRB and p53 through the inhibition of CDK4 and

CDK6. The predictive pathway from *Cdk7* suggests that CDK7 down-regulates *Ccna2*, *Egfr*, *Il1a*, *Mybl2*, *Nmyc1* and *Nras*, and up-regulates *Etv6*, *Figf*, *Pgf* and *Rbl1* (Fig. 2C). For the time course of the expression levels of *Cdk7*, *Ccna2*, *Egfr*, *Mybl2*, *N-myc* and *Nras* following the release from serum starvation, when the cells enter G1, the expression levels of *Cdk7* are reduced, resulting in the elevated expression of *Ccna2*, *Egfr*, *Mybl2*, *N-myc* and *Nras* (data not shown).

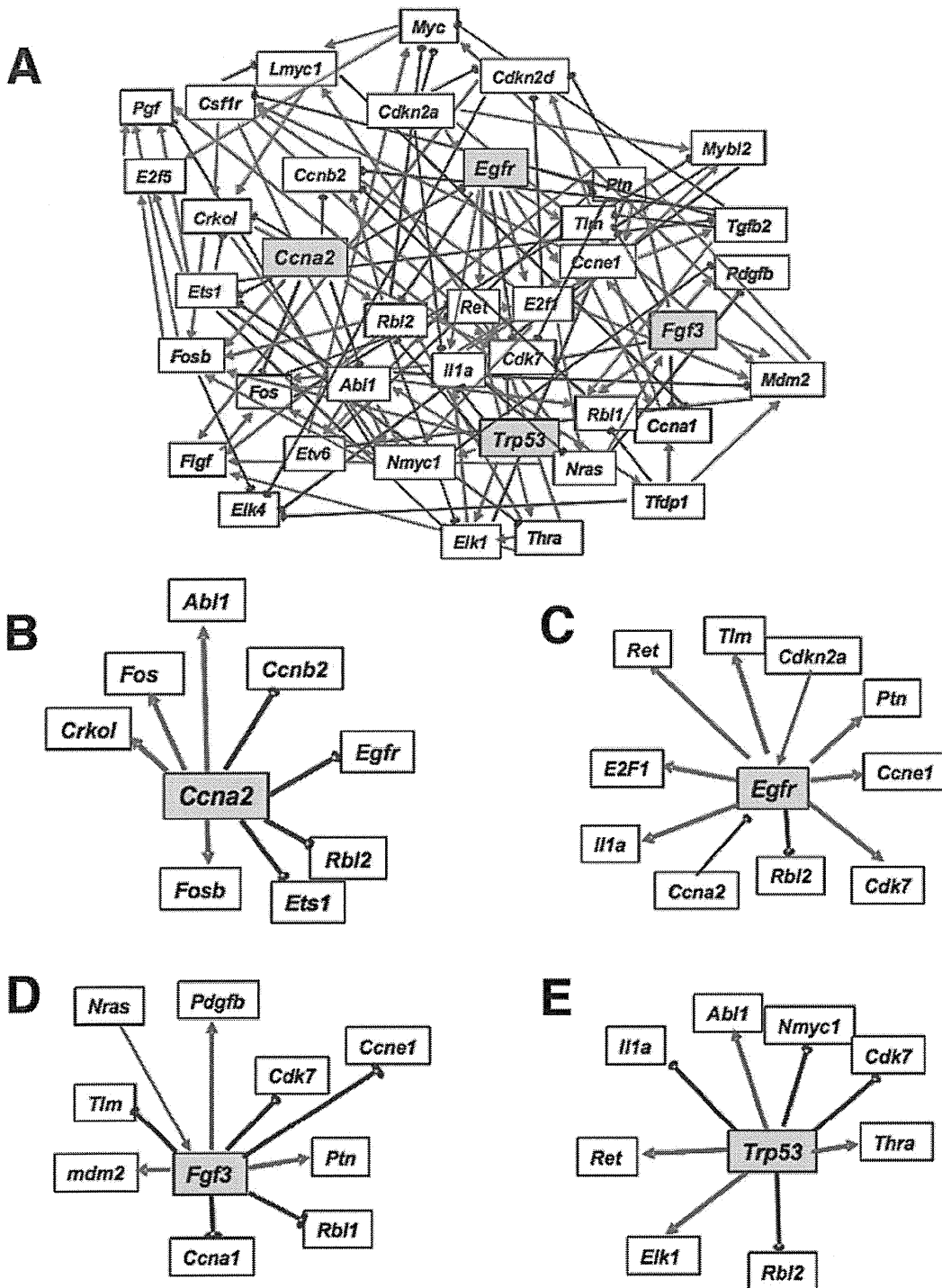


Fig. (3). Networks identified for the G1/S course data (A) and the isolated linkages associated with nodal genes Ccna2 (B), Egfr (C), Fgf3 (D) and Trp53 (E). Red arrows indicate linkages associated with upregulation and blue arrows indicate linkages associated with downregulation for any two genes within the network. Bold lines indicate linkages with nodal genes.

In the network found for the G1/S start data subset in hydroxyurea treated MEFs, the structure was observed to be more complicated and have no obvious central nodes. In this network, the number of connections from *Cdk7* and *Cdkn2a* to other genes was greatly decreased, whereas the connections from *Ccna2*, *Egfr*, *Fgf3*, *Trp53*, *Nmyc1*, *Ptn*, and *Rbl2* were increased (Fig. 3A). These changes suggested that

growth factors, such as *Egfr*, *Fgf3*, and *Ptn*, and proliferation regulators, such as *Ccna2*, *Trp53*, and *Rbl2*, have more prominent roles during S phase progression (Fig. 3B-E). From these data, it becomes obvious that the gene networks which regulate the progression of the cell cycle completely differ between the G0-G1 and G1-S transitions.

Table 3. Number of Linkages Between the 39 Selected Genes Related to Cell Cycle Control in MEFs

Gene Name	G0 Course			G1/S Course		
	Outward	Inward	Total	Outward	Inward	Total
<i>Abl1</i>	8	1	9	6	2	8
<i>Ccna1</i>	1	2	3	1	4	5
<i>Ccna2</i>	0	4	4	8	0	8
<i>Ccnb2</i>	2	5	7	0	4	4
<i>Ccne1</i>	0	2	2	3	5	8
<i>Crkol</i>	0	4	4	1	4	5
<i>Csflr</i>	5	0	5	4	3	7
<i>E2f5</i>	2	3	5	1	3	4
<i>Egfr</i>	4	4	8	8	2	10
<i>Elk1</i>	0	3	3	2	4	6
<i>Elk4</i>	1	5	6	0	4	4
<i>Ets1</i>	6	3	9	6	2	8
<i>Etv6</i>	3	4	7	3	2	5
<i>Fgf3</i>	6	0	6	8	1	9
<i>Figf</i>	1	5	6	1	4	5
<i>Fos</i>	1	1	2	2	5	7
<i>Fosb</i>	5	4	9	3	5	8
<i>Il1a</i>	2	5	7	5	4	9
<i>Lmyc1</i>	3	1	4	2	3	5
<i>Mybl2</i>	1	4	5	2	3	5
<i>Myc</i>	3	1	4	2	5	7
<i>Nmyc1</i>	1	4	5	4	4	8
<i>Nras</i>	2	3	5	5	2	7
<i>Pdgfb</i>	3	0	3	0	3	3
<i>Pgf</i>	1	5	6	0	5	5
<i>Ptn</i>	1	3	4	4	5	9
<i>Ret</i>	1	4	5	0	5	5
<i>Tfdp1</i>	2	5	7	4	1	5
<i>Tgfb2</i>	4	3	7	5	2	7
<i>Thra</i>	3	3	6	4	2	6
<i>Tlm</i>	2	5	7	0	4	4
<i>E2f1</i>	6	0	6	7	3	10
<i>Trp53</i>	4	4	8	8	0	8
<i>Mdm2</i>	4	3	7	3	5	8
<i>Cdkn2a</i>	13	1	14	6	0	6
<i>Cdk7</i>	10	1	11	1	5	6
<i>Rbl1</i>	3	4	7	1	4	5
<i>Rbl2</i>	1	4	5	5	4	9
<i>Cdkn2d</i>	2	4	6	2	4	6

Name abbreviations of the genes analyzed in this study are as listed in Table 2.

Verification of the Quantified Network

Further analyses were conducted to determine the statistical significance of the linkages between our identified genes. To find the most prominent linkages between genes of the network from *Cdk7* and of the network from *Trp53*, the G0 course dataset and the G1/S course dataset obtained from MEFs treated with serum starvation or hydroxyurea were used, respectively. This analysis method can predict both the strength of the relationships between genes and the posterior distribution of parameters in the log-linear model [22, 23]. Of the 10 genes associated with *Cdk7*, 9 had some posterior densities that did not include 0, suggesting very significant associations (Table 4). Only *Il1a* included 0 in the posterior density, with 18% of the distribution above zero and 82% below. This finding suggested a statistically marginal down-regulation. Fig. (4) illustrated the distribution for a strong down-regulation (*Cdk7* → *Nras*) and for a weak down-regulation (*Cdk7* → *Il1a*). A negative association between *Nras* and *Cdk7* has been reported previously [28], suggesting that the method we employed in our present analyses can extract negative relationships between two genes using simple microarray data.

Table 4. Summary of the Results from the MCMC Analyses

Parent	Target	Mean	Std.	Percent <0
G0 Network				
Cdk7	<i>Ccna2</i>	-6.0037	0.0718	0
	<i>Egfr</i>	-2.5725	0.0265	0
	<i>Etv6</i>	2.0637	0.0279	0
	<i>Figf</i>	1.4832	0.0022	0
	<i>Il1a</i>	-1.0015	1.0882	17.9
	<i>Mybl2</i>	-2.8674	0.0141	0
	<i>Nmyc1</i>	-0.712	0.0064	0
	<i>Nras</i>	-2.8768	0.0626	0
	<i>Rgf</i>	6.7274	0.0059	0
	<i>Rbl1</i>	1.9701	0.0065	0
G1 Network				
P53	<i>Abl1</i>	0.9456	0.4592	0.0225
	<i>Cdk7</i>	-3.7324	0.0008	0
	<i>Elk1</i>	6.7449	1.3828	0.004
	<i>Il1a</i>	-1.5102	0.0721	0
	<i>Nmyc1</i>	6.1901	0.0417	0
	<i>Rbl1</i>	-6.6934	0.3521	0
	<i>Ret</i>	1.7052	2.7057	25.7

For G0 data, MCMC sampling was performed 140,000 times and the mean, standard deviation (Std.) and percentage below zero were assessed from the last 70,000 samplings. If the number was negative, only the samples above zero were counted. For G1 data, MCMC sampling was performed 300,000 times and the mean, Std., and percentage below zero were assessed from the last 150,000 samplings.

In the G1/S network, *Trp53* suppressed the expression of *Cdk7* and *Rbl2*, and stimulated that of *Abl1*, *Il1a*, *Nmyc*, *Elk1*, *Ret* and *Thra* (Fig. 3E). *Trp53* has previously been

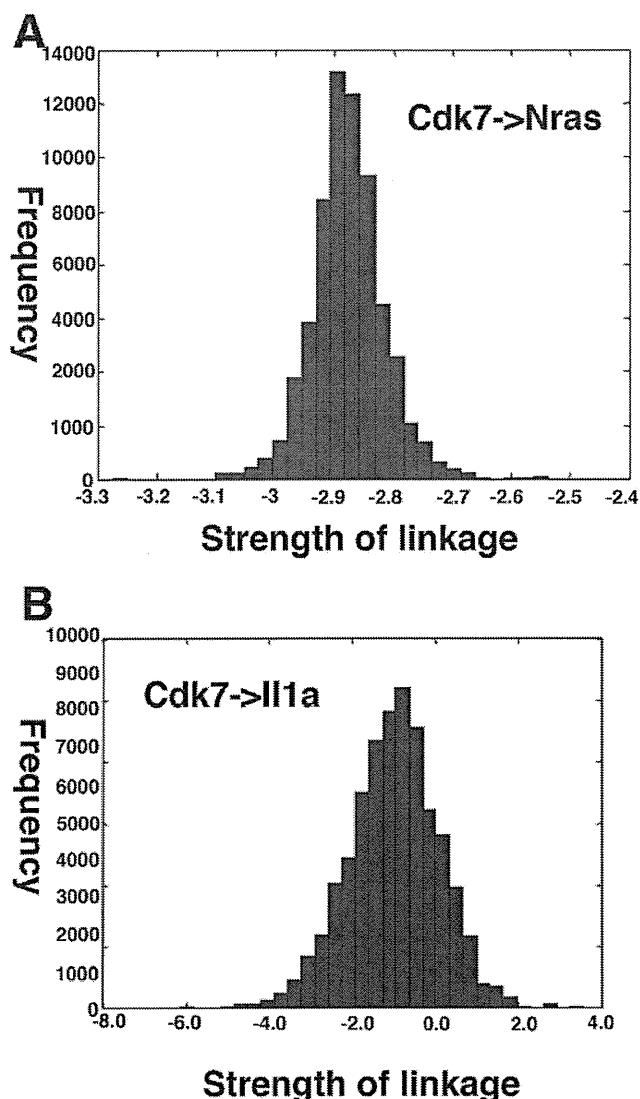


Fig. (4). (A, B) Frequency histograms approximating the posterior distributions for linkages from Cdk7 to Nras (a statistically significant downregulation) and Cdk7 to Il1a (marginally significant downregulation). Histograms were derived by Bayesian analysis of the gene interaction network shown in Fig. (2C) using 70,000 out of 140,000 Markov-Chain Monte Carlo samples and prior distributions as shown in Table 4.

shown to negatively regulate cyclinD/CDK4, cyclinD/CDK6, cyclinB/cdk2, and cyclinA/cdk2 through the activation of p21 in normal cells. CyclinD/CDK4/6 on the other hand activates phosphorylated RB (pRb) which leads to the activation of E2F, which in turn negatively regulates p53 through p19^{ARF} activation and MDM2 suppression [1, 29]. The interaction between p53 and c-Abl is known to play a critical role in the cell growth and G1 arrest response to DNA damage under normal conditions [30]. It has been reported that CDK7 phosphorylates other CDKs, which is an essential step for their activation [31] and that a direct involvement of p53 in triggering growth arrest by its interaction with the CDK activating kinase complex [32]. These reports and our predictive network suggest therefore that CDK7 is essential for mitosis.

Detection of Gene Networks Using a Recombinant Mouse CDK7 Retrovirus System

Our cell cycle network data indicated that CDK7 activation negatively regulates the expression of *Egfr* and *Nmyc1* in MEFs. To validate this observation, we introduced mouse CDK7 into these cells using a recombinant retrovirus system to evaluate negative regulation of CDK7 against EGFR and N-MYC. The titer of the retrovirus obtained from PT67 producer cells was 4.0×10^9 virus copies/ml for the LXIN empty vector and 5.4×10^9 virus copies/ml for the CDK7 recombinant retrovirus. The hemagglutinin (HA) protein tag was added to the carboxyl terminus of recombinant CDK7 so that we could distinguish the recombinant protein from its endogenous counterpart.

As shown in Fig. (5), western blot detection with a HA antibody revealed the expression of recombinant CDK7 protein in infected MEF cells. Increased levels of total CDK7 protein (endogenous plus recombinant CDK7) was also confirmed by immunoblotting with a CDK7 antibody (Fig. 5A). The EGFR, N-MYC1 and c-FOS protein levels detected by western blot were decreased in MEF cells infected with the CDK7-expressing retrovirus when compared with the control cells (Fig. 5A). c-FOS was used as control because there was no direct linkage between CDK7 and c-FOS (see Fig. 2A). The average levels of EGFR and N-MYC1 from three separate experiments are shown in Fig. (5B). Decreased EGFR and N-MYC1 but not c-FOS protein levels indicated that the exogenous introduction of CDK7 negatively influenced their expression. From these results, we concluded that one part of our newly detected cell cycle network had been validated.

DISCUSSION

Gene set enrichment is one means of providing reliable information about specific basic biological processes and has been the most widely used gene-set analysis method to date [33-36]. Directed graphical models known as Bayesian networks, and the MCMC method of determining network inference, have been shown to be promising approaches to obtaining new information about gene networks in various tissues and cells.

In our current study, we adopted an approach based on a systematic analysis of gene expression data to define a gene regulatory network and new putative CDK7 functions were identified by quantifying the dynamics of the gene regulatory networks for cell cycle control in MEF cells. A previous study has suggested that a TFIID complex containing CDK7 is responsible for the phosphorylation of CDK2 and CDK4, both of which are crucial contributors to the G1/S cell cycle transition in human and mouse cells [37]. One of the TFIID components critically regulates the CAK activity of CDK7 during mitotic progression, suggesting that mitotic silencing of basal transcription is important to the *Drosophila* cell cycle [38]. The previous study indicated that the phosphorylation of CDK7 cause the inhibition of TFIID-associated kinase and transcriptional activity [39]. Although we do not have any data about the phosphorylation status of introduced recombinant CDK7 protein, there is a possibility that the extra amount of CDK7 protein resulted in the reduced transcriptional activity of TFIID. The gene networks

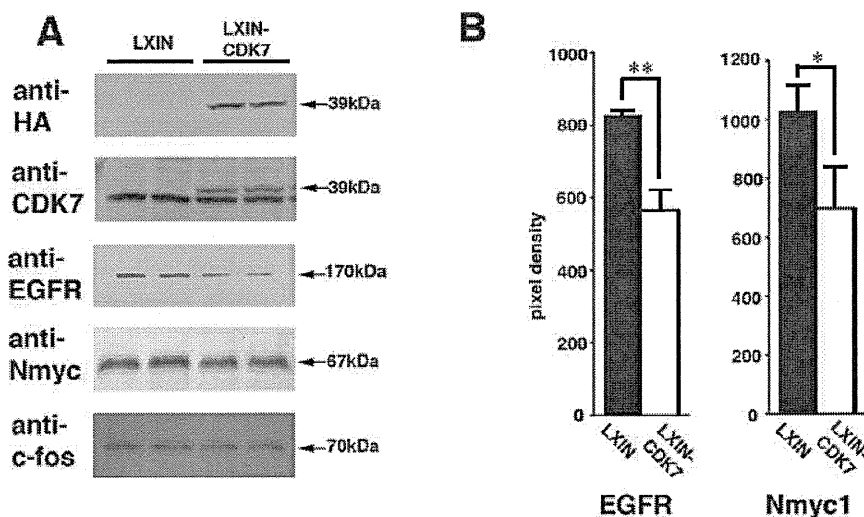


Fig. (5). Experimental verification of detected gene network from Cdk7 to EGFR and N-myc1 using a recombinant retrovirus expression system. **(A)** The protein levels of exogenous Cdk7 (HA), total Cdk7 (Cdk7), EGFR, and N-myc1 were detected by western blotting. Representative blots obtained from two independent samples are shown in the figure. **(B)** EGFR and N-myc1 protein levels were quantitatively analyzed. Data are the average plus standard deviation of 6 western blots from two independent samples for each group. *, $P < 0.05$; **, $P < 0.01$.

found in this study have to be further evaluated in terms of whether they are based on direct or indirect interactions, however, this is to our knowledge the first report showing the importance of CDK7 associated networks for the progression from G0 to G1.

We also analyzed gene networks associated with S phase and M phase, in addition to the progression from G0 to G1, which focused in our current linkage analysis. Several central nodes were detected but their networks will need to be further evaluated experimentally, as shown for CDK7 in this study. We thus reveal that the qualitative algorithm based on Bayesian networks is a useful tool for detecting gene networks that function at specific phases of the cell cycle. Our results indicate that CDK7 negatively regulates EGFR and N-myc expression to control G1 entry. When the MEF cells do enter G1 from G0, the expression of *Cdk7* is suppressed, resulting in the increased expression of the *Egfr* and *N-myc* genes and protein products. EGFR is known act as a growth factor receptor, and activated EGFR is known to promote cell cycle progression through the G1-related Cyclin complex. N-myc is also known to stimulate cell proliferation and CDK7 thus appears to act as a negative regulator of cell proliferation and cell cycle progression in mammalian cells.

Although the CAK activation at the G1/S phase transition promotes mitotic progression, the relationship between *Cdk7* and *Egfr* was observed at the G0/G1 phase but not the G1/S phase in our case. When we looked for the relationship between two genes at the database GEO (<http://www.ncbi.nlm.nih.gov/sites/GDSbrowser>) for confirming our data, the relationships are reversal at the early stage after several treatments of serum starvation, cat or Campthothecin. This public evidences can support our data, implicating that CDK7 regulates EGFR expression levels according to the type of cell cycle stage.

Our study detected the gene networks from CDK7 to the downstream. As the next step for the study, these inhibitory effects would be needed to analyze from the viewpoint of kinetics. The kinetics study would explore how fast the transcriptional inhibition reaches to the equilibrium in the process of the cell cycle. The time course analysis with the efficient inducible expression system of recombinant CDK7 would be required to get these data.

Whereas our overall approach in this study was based upon a specific set of tools, other tools could be used to obtain similar findings. Gene ontology was used to select specific genes to consider when defining the network. Other classification methods however, such as clustering, could have also been used to select a specific gene group. Sequence/structure analysis of transcription factors in order to verify gene nodes could be replaced by analyses of protein structure, protein-protein interactions, or protein-DNA interactions. The log-linear mathematical model used to quantify gene interactions could easily be replaced by mechanism-based dynamic models if the data could support more parameters. However, the simplicity of the model used in this analysis has the advantage of providing rapid identification of gene relationships that are helpful in elucidating the structure and dynamics of the gene network using only gene expression profiles. With only one parameter in the model for each gene-gene relationship, one can more easily visualize and understand complex network relationships.

We validated part of our predicted network with a retrovirus CDK7 expression system. The exogenous introduction of mouse CDK7 into MEF cells caused a decrease in the protein levels for EGFR and N-MYC1. These findings provided supporting evidence for the validity of our detected gene network. The molecular weight of the retroviral CDK7 was slightly higher than the endogenous

protein in mouse MEF cells. According to the Genbank database, there is an alternative splice site at the position of exon 6 in CDK7 (accession number: NMV009874.3). Although our cloned CDK7 is the most common form (346aa, 38.9kDa, accession number: NMV009874), and was mainly used in previous functional studies, there is a possibility that endogenous CDK7 expressed in MEF cells is a short form of this protein that arises through the alternative splicing of exon 6. We predict that there is no functional difference between the short form of CDK7 and our recombinant version, since the binding site of MAT7 and phosphorylation sites are present in both forms.

To further test the negative regulatory relationship between CDK7 and EGFR or N-MYC, we attempted to knockdown endogenous CDK7 using a siRNA approach and also a Cre-loxP mediated conditional expression system. However, neither approach was successful in the MEF cells due to a low transfection efficiency for siRNA and the cell toxicity of the adenovirus which expresses the Cre recombinase.

Another important factor to consider is the condition of the MEFs. We used cells that were not immortalized, which allowed us to investigate gene network dynamics in a normal cell context. However, such cells are severely limited in their replicative capacity, resulting in a limited number of applicable approaches for genetic manipulation. Since the inactivation of both p16 and p53 has previously been reported to be essential for the immortalization of MEFs, it is almost certain that the entire cell cycle network would be severely affected by the immortalization process.

An important objective in Bayesian network learning is to infer the network topology. We used 39 genes based on MAP criterion in this study. Even with 39 genes, the topology space is 2^{39} . However, it is difficult (virtually impossible) to conclude that the optimized network is the best one without doing all possible topologies, an impossibility for 2^{39} topologies. Therefore, a search algorithm, described with step-by-step instructions in the previous work [21], was used to obtain a network topology. Also in the previous work [21], a series of simulation studies were undertaken to address the operating characteristics of the algorithm and to determine the conditions under which it would fail. The analysis used a simple log-linear model to infer linkages in the network. The approach used has advantages and disadvantages over other approaches. The major advantage is a compact parameter space using the minimum number of parameters to infer the network that allows us to use a single parameter to infer the strength of a linkage. This also reflects on the major disadvantage in that it is not possible to use this model to describe the dynamics of the interactions *per se* as such a mechanistic model would require more complex biomathematical descriptions of each linkage and considerably more data. That said simple linear models have been a mainstay of descriptive statistical evaluations of biological data for decades. In this case, they allow us to test the hypothesis of no linkage between genes against the alternative of a proportionate change on a log-scale and infer linkage.

The analysis tool used here is able to find genes that appear to be positively or negatively correlated as the gene expression patterns change over time. If a gene is only

changed at one time, say 6 hours, and its target genes are only altered at a different time, say 12 hours, this algorithm would be unlikely to identify the linkage. A dynamic model, describing the patterns over time in a more mechanistic fashion, might locate such a linkage, although it might still be very difficult. For the data being examined here, it is more likely that the dynamic changes in gene expression occur gradually throughout the course of the experiment (18-24 hours) resulting in correlations through time that can be observed in our simple linear model.

In summary, the results of our network analyses have raised a number of new possibilities concerning the roles of numerous genes in the regulation of the murine cell cycle. The limitations of these analyses (use of only microarray data, a simple log-linear model, and promoter region sequences) preclude a stronger interpretation of the results. However, as additional data are obtained in future studies that address the hypothetical linkages identified by our findings, it should be possible to bring them formally into an improved analysis and critically evaluate each linkage in greater detail. This is the overall goal of cancer systems biology and the general approach presented here should form the basis for future attempts at system-wide analyses of biological function.

ACKNOWLEDGEMENTS

We thank Leping Li, Delong Liu, Rick Paules, David Umbach, Scott Auerbach and Ben Van Houten (NIH/NIEHS) for their comments on this work, and J. R. Nevins and S. Ishida for kindly providing the original dataset. This research was supported in part by the National Institute of Environmental Health Sciences.

SUPPLEMENTAL MATERIALS

This article also contain supplementary material and it can be viewed at publisher's website along with the article.

REFERENCES

- [1] Sears RC, Nevins JR. Signaling networks that link cell proliferation and cell fate. *J Biol Chem* 2002; 277: 11617-20.
- [2] Stillman B. Cell cycle control of DNA replication. *Science* 1996; 274: 1659-64.
- [3] Cho RJ, Huang M, Campbell MJ, *et al.* Transcriptional regulation and function during the human cell cycle. *Nat Genet* 2001; 27: 48-54.
- [4] Ishida S, Huang E, Zuzan H, *et al.* Role for E2F in control of both DNA replication and mitotic functions as revealed from DNA microarray analysis. *Mol Cell Biol* 2001; 21: 4684-99.
- [5] Iyer VR, Eisen MB, Ross DT, *et al.* The transcriptional program in the response of human fibroblasts to serum. *Science* 1999; 283: 83-7.
- [6] Haller F, Gunawan B, von Heydebreck A, *et al.* Prognostic role of E2F1 and members of the CDKN2A network in gastrointestinal stromal tumors. *Clin Cancer Res* 2005; 11: 6589-97.
- [7] Katoh Y, Katoh M. Identification and characterization of DISP3 gene *in silico*. *Int J Oncol* 2005; 26: 551-6.
- [8] Tonon G. From oncogene to network addiction: the new frontier of cancer genomics and therapeutics. *Future Oncol* 2008; 4: 569-77.
- [9] Emmert-Streib F, Dehmer M. Predicting cell cycle regulated genes by causal interactions. *PLoS One* 2009; 4: e6633.
- [10] Margolin AA, Califano A. Theory and limitations of genetic network inference from microarray data. *Ann N Y Acad Sci* 2007; 1115: 51-72.
- [11] Djebbari A and Quackenbush J: Seeded Bayesian Networks: constructing genetic networks from microarray data. *BMC Syst Biol* 2: 57, 2008.

- [12] Gevaert O, De Smet F, Kirk E, *et al.* Predicting the outcome of pregnancies of unknown location: Bayesian networks with expert prior information compared to logistic regression. *Hum Reprod* 2006; 21: 1824-31.
- [13] Nakayama KI, Nakayama K. Ubiquitin ligases: cell-cycle control and cancer. *Nat Rev Cancer* 2006; 6: 369-81.
- [14] Nourse J, Firpo E, Flanagan WM, *et al.* Interleukin-2-mediated elimination of the p27Kip1 cyclin-dependent kinase inhibitor prevented by rapamycin. *Nature* 1994; 372: 570-3.
- [15] Reynisdottir I, Polyak K, Iavarone A, *et al.* Kip/Cip and Ink4 Cdk inhibitors cooperate to induce cell cycle arrest in response to TGF-beta. *Genes Dev* 1995; 9: 1831-45.
- [16] Susaki E, Nakayama K, Nakayama KI. Cyclin D2 translocates p27 out of the nucleus and promotes its degradation at the G0-G1 transition. *Mol Cell Biol* 2007; 27: 4626-40.
- [17] Susaki E, Nakayama KI. Multiple mechanisms for p27(Kip1) translocation and degradation. *Cell Cycle* 2007; 6: 3015-20.
- [18] Tanaka A, Muto S, Konno M, *et al.* A new IkappaB kinase beta inhibitor prevents human breast cancer progression through negative regulation of cell cycle transition. *Cancer Res* 2006; 66: 419-26.
- [19] Matsumoto G, Namekawa J, Muta M, *et al.* Targeting of nuclear factor kappaB Pathways by dehydroxymethylepoxyquinomicin, a novel inhibitor of breast carcinomas: antitumor and antiangiogenic potential *in vivo*. *Clin Cancer Res* 2005; 11: 1287-93.
- [20] Elangovan S, Hsieh TC, Wu JM. Growth inhibition of human MDA-mB-231 breast cancer cells by delta-tocotrienol is associated with loss of cyclin D1/CDK4 expression and accompanying changes in the state of phosphorylation of the retinoblastoma tumor suppressor gene product. *Anticancer Res* 2008; 28: 2641-7.
- [21] Yamanaka T, Toyoshiba H, Sone H, *et al.* The TAO-Gen algorithm for identifying gene interaction networks with application to SOS repair in *E. coli*. *Environ Health Perspect* 2004; 112: 1614-21.
- [22] Toyoshiba H, Sone H, Yamanaka T, *et al.* Gene interaction network analysis suggests differences between high and low doses of acetaminophen. *Toxicol Appl Pharmacol* 2006; 215: 306-16.
- [23] Toyoshiba H, Yamanaka T, Sone H, *et al.* Gene interaction network suggests dioxin induces a significant linkage between aryl hydrocarbon receptor and retinoic acid receptor beta. *Environ Health Perspect* 2004; 112: 1217-24.
- [24] Dahlquist KD, Salomonis N, Vranizan K, *et al.* GenMAPP, a new tool for viewing and analyzing microarray data on biological pathways. *Nat Genet* 2002; 31: 19-20.
- [25] Fukuda T, Mishina Y, Walker MP, *et al.* Conditional transgenic system for mouse aurora a kinase: degradation by the ubiquitin proteasome pathway controls the level of the transgenic protein. *Mol Cell Biol* 2005; 25: 5270-81.
- [26] Nigg EA. Cyclin-dependent kinase 7: at the cross-roads of transcription, DNA repair and cell cycle control? *Curr Opin Cell Biol* 1996; 8: 312-7.
- [27] Schulze A, Zerfass K, Spitkovsky D, *et al.* Activation of the E2F transcription factor by cyclin D1 is blocked by p16INK4, the product of the putative tumor suppressor gene MTS1. *Oncogene* 1994; 9: 3475-82.
- [28] Abdellatif M, Packer SE, Michael LH, *et al.* A Ras-dependent pathway regulates RNA polymerase II phosphorylation in cardiac myocytes: implications for cardiac hypertrophy. *Mol Cell Biol* 1998; 18: 6729-36.
- [29] Ball KL. p21: Structure and Functions Associated with Cyclin-cdk Binding. In: L Meijer, Guidet, S., Philippe, M. (ed.), *Progress in cell cycle research*: Plenum press, New York, Vol. 3, pp. 125. 1997.
- [30] Sionov RV, Coen S, Goldberg Z, *et al.* c-Abl regulates p53 levels under normal and stress conditions by preventing its nuclear export and ubiquitination. *Mol Cell Biol* 2001; 21: 5869-78.
- [31] Larochelle S, Pandur J, Fisher RP, *et al.* Cdk7 is essential for mitosis and for *in vivo* Cdk-activating kinase activity. *Genes Dev* 1998; 12: 370-81.
- [32] Schneider E, Montenarh M, Wagner P. Regulation of CAK kinase activity by p53. *Oncogene* 1998; 17: 2733-41.
- [33] Subramanian A, Tamayo P, Mootha VK, *et al.* Gene set enrichment analysis: a knowledge-based approach for interpreting genome-wide expression profiles. *Proc Natl Acad Sci U S A* 2005; 102: 15545-50.
- [34] Goeman JJ, Buhlmann P. Analyzing gene expression data in terms of gene sets: methodological issues. *Bioinformatics* 2007; 23: 980-7.
- [35] Mootha VK, Lindgren CM, Eriksson KF, *et al.* PGC-1alpha-responsive genes involved in oxidative phosphorylation are coordinately downregulated in human diabetes. *Nat Genet* 2003; 34: 267-73.
- [36] Toyoshiba H, Sawada H, Naeshiro I, *et al.* Similar compounds searching system by using the gene expression microarray database. *Toxicol Lett* 2008.
- [37] Watanabe Y, Fujimoto H, Watanabe T, *et al.* Modulation of TFIIH-associated kinase activity by complex formation and its relationship with CTD phosphorylation of RNA polymerase II. *Genes Cells* 2000; 5: 407-23.
- [38] Chen J, Larochelle S, Li X, *et al.* Xpd/Erc2 regulates CAK activity and mitotic progression. *Nature* 2003; 424: 228-32.
- [39] Akoulitchev S, Reinberg D. The molecular mechanism of mitotic inhibition of TFIIH is mediated by phosphorylation of CDK7. *Genes Dev* 1998; 12: 3541-50.

Received: May 11, 2009

Revised: February 1, 2010

Accepted: March 1, 2010

© Sone *et al.*; Licensee Bentham Open.This is an open access article licensed under the terms of the Creative Commons Attribution Non-Commercial License (<http://creativecommons.org/licenses/by-nc/3.0/>) which permits unrestricted, non-commercial use, distribution and reproduction in any medium, provided the work is properly cited.